Saccharin disrupts the bacterial cell envelope stability and interferes with DNA replication dynamics.

Rubén de Dios[1], Kavita Gadar[1], Chris R Proctor[1], Evgenia Maslova[1], Jie Han[1], Dominika Krawiel[1],Emma L. Dunbar[6], Bhupender Singh[3], Stelinda Peros[2], Tom Killelea[4], Anna-Luisa Warnke[5], Marius M Haugland[5], Edward L. Bolt[4], Christian S. Lentz[3], Christian J. Rudolph[2], Ronan R McCarthy[1]

[1] [A]Antimicrobial Innovations Centre, Division of Biosciences, Department of Life Sciences, College of Health, Medicine and Life Sciences, Brunel University London, Uxbridge, UB8 3PH, UK.

[2] Division of Biosciences, Department of Life Sciences, Centre for Genome Engineering and Maintenance, College of Health, Medicine and Life Sciences, Brunel University London, Uxbridge, UB8 3PH, UK.

[3] Research Group for Host-Microbe Interactions, Department of Medical Biology and Centre for New Antibacterial Strategies (CANS), UiT—The Arctic University of Norway, 9019 Tromsø, Norway

[4] School of Life Sciences, Faculty of Medicine & Health Sciences, Queens Medical Centre, University of Nottingham, NG7 2UH, UK

[5] Department of Chemistry, UiT—The Arctic University of Norway, 9037 Tromsø, Norway

[6] Department of Biochemistry, University of Wisconsin-Madison, Madison, WI 53706-1544, USA

Abstract.

Saccharin has been part of the human diet for over 100 years and there is a comprehensive body of evidence demonstrating that it can influence the gut microbiome, ultimately impacting human health. However, the precise mechanisms through which saccharin can impact bacteria have remained elusive. In this work, we demonstrate that saccharin inhibits cell division, leading to a cell filamentation with altered DNA synthesis dynamics.We show that these effects on the cell are superseded by the formation of bulges emerging from the cell envelope which ultimately trigger in cell lysis.. We demonstrate that saccharin can inhibit the growth of both Gram-negative and Gram-positive bacteria as well as disrupt key phenotypes linked to host colonisation, such as motility and biofilm formation. Additionally, we test its potential to disrupt established biofilms (single-species as well as polymicrobial) and its capacity to resensitise multidrug resistant pathogens to last resort antibiotics. Finally, we present *in vitro* evidence on the versatility of saccharin as a potential antimicrobial by integrating it into an effective hydrogel wound dressing.

Introduction

The critical rise in global obesity has led to a progressive increase in the consumption of non-caloric artificial sweeteners worldwide. Currently, it is estimated that 25% of children and 41% of adults in the United States are daily consumers of artificial sweeteners (Sylvetsky *et al*., 2017). Among the most popular artificial sweeteners, saccharin has become the market leader in relation to its sweetening power (Sylvetsky and Rother, 2016). Saccharin ($C_7H_5NO_3S$) is a heat-stable artificial sweetener that is approximately 300-700 times sweeter than sucrose. In contrast, it has a zero net caloric contribution to the diet. It was first discovered by accident in the late 1870s by a chemist, Constantin Fahlberg, who noted an intense sweet taste on his hand while working on the development of benzoic sulfimide coal tar derivatives (Sylvetsky and Rother, 2016). The sweetener was quickly commercialized and grew in popularity particularly, during World War I, when traditional sugar was in short supply. Its proliferation into the human diet was further accelerated in the 1960s, as it was marketed as a product to support weight loss.

The impact of artificial sweeteners on the host microbiome has become an increasingly emergent area of focus. The effect of saccharin on the gut microbiome was first reported in 1980, when male rats were fed 7.5% saccharin for 10 days. Although it showed no impact on the total anaerobe numbers in the caecum, specific sub-populations of anaerobes were depleted (Anderson and Kirkland, 1980). More recently, Suez *et al*. (2014) established a link between saccharin consumption and glucose intolerance via alterations in the gut microbiota (Suez *et al*., 2014). However, a later study exploring the effects of saccharin on the gut microbiota and glucose

tolerance in healthy mice and humans demonstrated no impact on the glucose or hormonal responses. No major impacts on the microbiome composition of either mice or humans were reported, although some minor shifts at the genus level were noted in mice (Serrano *et al*., 2021). Interestingly, while several additional studies have pointed towards an impact of sweeteners, including saccharin, on the microbiome, there appears to be a lack of a consistent signature across these studies that could be used as a marker of artificial sweetener consumption. Nevertheless, it has been reported that artificial sweeteners, including saccharin, can trigger inflammatory responses by different means. Bian *et al.* (2017) gave mice saccharin via drinking water (0.3 mg/ml) and found that this induced gut microbiome alterations that coincided with an increase in pro-inflammatory mediators. Moreover, Skurk *et al*. (2023) demonstrated that saccharin, at similar concentrations to those expected in plasma after dietary intake, produced alterations in the transcriptional signature of neutrophils. This led to a shift in their state from "homeostasis" to "priming", thus promoting inflammation. In contrast to this, other reports have shown that saccharin derivatives can inhibit other immune pathways leading to inflammation and have even been proposed as antagonists to modulate interferon-mediated inflammation (Csakai *et al*., 2014). This points towards a highly specific effect of saccharin on the microbiome, but a multifactorial effect on the host, specifically on the immune system, which would altogether be heavily influenced by the host diet and lifestyle.

The effect at the microbiome level has received much attention, but the impact of saccharin on specific bacterial species at the cellular level is less clear. However, there is a mounting body of evidence that saccharin can influence bacterial growth, including an inhibition of members of the oral microbiome, such as *Porphyromonas gingivalis and Aggregatibacter actinomycetemcomitans* (Prashant *et al*., 2012). Similarly, it has been shown to limit the growth of a range of lab model

bacteria including *Staphylococcus aureus, Bacillus cereus, Klebsiella pneumoniae* and *Pseudomonas aeruginosa* (Sünderhauf *et al*., 2020, Wang *et al*., 2018). Furthermore, saccharin has been shown to influence natural transformation in a range of environmental bacterial species (Yu *et al.*, 2021, Yu *et al.*, 2022). Recent work has also demonstrated that saccharin, along with other artificial sweeteners such as acesulfame-K (ace-K), can inhibit the growth of multidrug-resistant (MDR) *P. aeruginosa* and *Acinetobacter baumannii* (de Dios *et al*., 2023), the later occupying the first position on the World Health Organisation (WHO) priority pathogen list (Tacconelli *et al*., 2018).

Despite this mounting body of evidence, the mechanisms underpinning saccharin-mediated growth inhibition in bacteria remains unexplored. In this work, we provide direct evidence for the first time that saccharin can produce bulge-mediated cell lysis leading to cell death and alter DNA synthesis dynamics within the cell. We provide proof-of-concept results for the use of saccharin as an antimicrobial and anti-virulence therapeutic in a range of MDR bacteria. Apart from the direct antimicrobial effect of this artificial sweetener, we demonstrate that saccharin disrupts the cell envelope as a barrier. This facilitates a greater antibiotic penetration and overwhelms native resistance mechanisms in MDR *A. baumannii*, thus re-sensitising it to frontline antibiotics. As a final step, we demonstrate the therapeutic potential of saccharin as an antimicrobial in *in vitro* and *ex vivo* models.

Results

Saccharin induces filamentation and bulge mediated cell lysis.

Saccharin has previously been reported to have antimicrobial activity (Sunderhauf *et al.,* 2020, Yu *et al.,* 2022, Yu and Guo, 2022, de Dios *et al*., 2023), although the mechanisms underpinning this activity have remained elusive. To understand how the cell responds to saccharin exposure, we performed time-lapse microscopy using an *E. coli* model and treating with 1.4% saccharin, an effective concentration tested empirically in this setting and close to the theoretical half-maximal inhibitory concentration (IC50) (Figure 1A, Supplementary Figure S1). In this setup, we could see that cells acquired an aberrant morphology, filamenting and swelling in the central section. As the treatment progresses, membrane bulges also appear and continue to grow. Eventually, this led to cell lysis, with the concomitant emergence of a "ghost" cell (Supplementary Video S1, Supplementary Video S2). This bulge mediated cell lysis is remarkably similar to the morphological response we previously reported for cells when exposed to the sweetener ace-K (de Dios *et al*., 2023), suggesting a similar mechanism of action. Using the cardiolipin (CL)-specific fluorescent dye 10-N-nonyl-acridine orange (NAO) to visualise CL distribution, we could see clear structural rearrangements in the cell membrane, which align with previous reports of saccharin altering the membrane integrity and permeability (Yu *et al,* 2021, Yu *et al.,* 2022, Yu and Guo, 2022), and confirm that the bulges were emerging from cells prior to lysis (Mileykovskaya & Dowhan, 2000).

To gain more insights on how saccharin may interfere with cell division, we performed a differential staining at multiple timepoints after saccharin treatment with an *E. coli* strain bearing an eCFP-labelled version of *ftsZ*. This allowed us to track the progression of the membrane status over time, as well as septation (Figure 1B). The membrane staining re-confirmed the loss of

morphological integrity and the formation of bulges after saccharin treatment. FtsZ rings could clearly be seen forming in the cells indicating that the impact of saccharin on cell division was not due to the inhibition of septum formation but could be due to these septa being prevented or

142 blocked from completing fission.

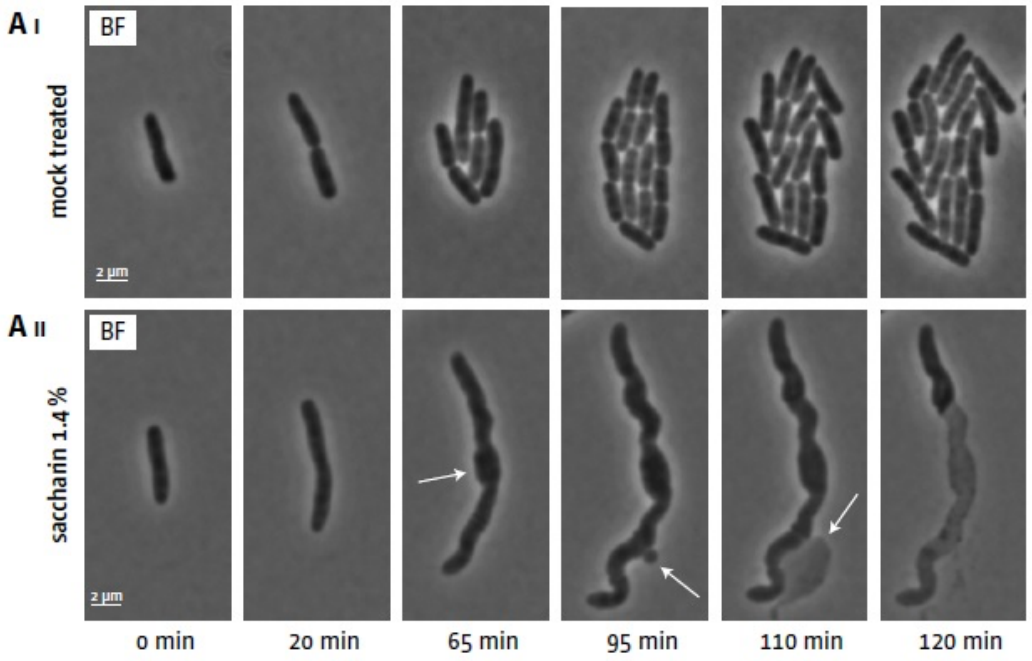
A I
BF
mock treated
2 µm
A II
BF
saccharin 1.4 %
2 µm
0 min
20 min
65 min
95 min
110 min
120 min

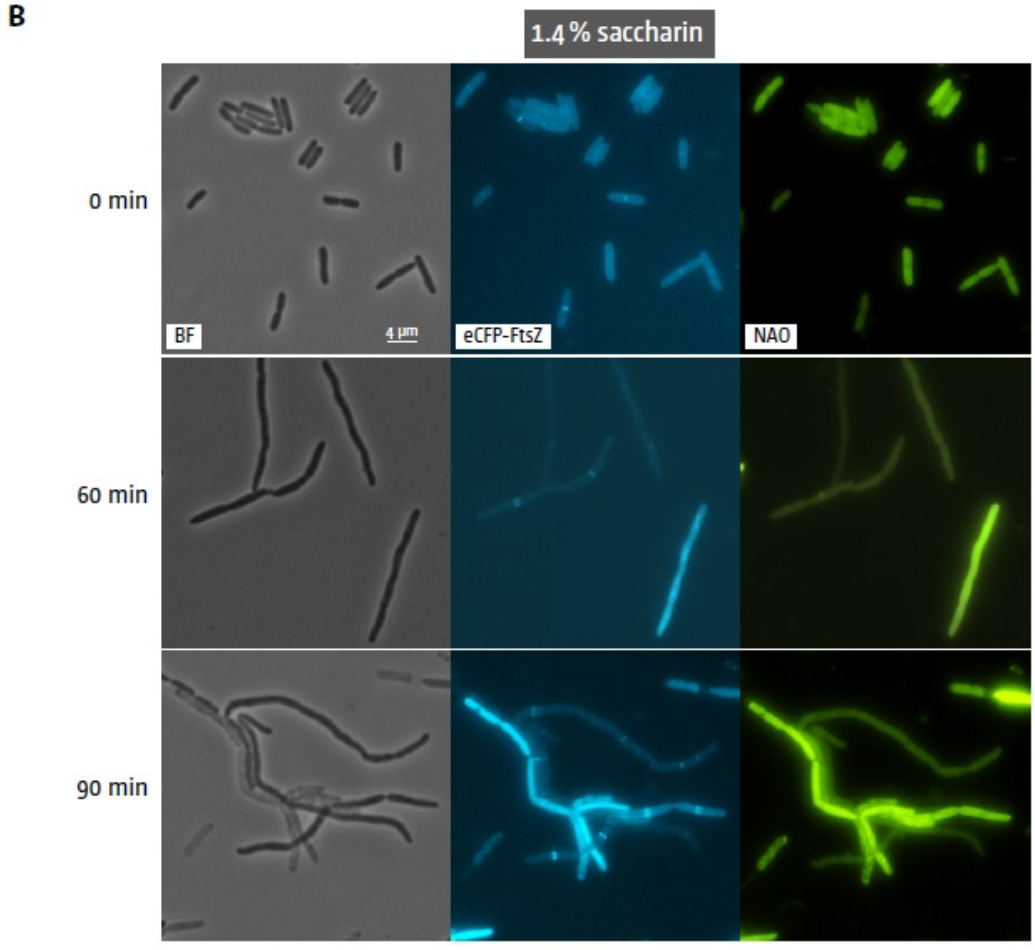
B
1.4 % saccharin
0 min
60 min
90 min
BF
4 µm
eCFP-FtsZ
NAO

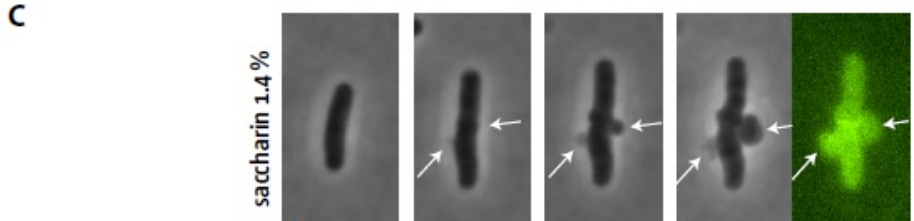
C
saccharin 1.4 %

Figure 1: Impact of saccharin on cellular growth and morphology. **Ai-ii**) Phase contrast images of a time lapse of *E. coli* MG1655 cells mock treated (i) and treated with 1.4% saccharin (ii). An environmental chamber was used to maintain a constant temperature of 37 °C and cells imaged for 120 min. The images shown highlight the formation of a membrane bulge (white arrows), which quickly becomes so extensive that it ruptures, leaving a "ghost" behind. **B**) Phase contrast and fluorescent images of *E. coli* cells following treatment with saccharin. Cells were grown in LB broth (Miller) to early exponential growth phase. Aliquots were transferred to pre-warmed culture tubes and saccharin added at the concentration indicated. Samples were taken at the time shown. The membrane was visualised by staining with 10-nonyl acridine orange (NAO) for 5 min before visualisation (see Material and Methods for details). Septum formation was visualised by expressing a FtsZ allele fused to CFP (see Material and Methods details) C) Time lapse of 1.4% saccharin-induced cell envelope bulging with NAO bulge staining. Shown are representative images from a minimum of three biological replicates.

Saccharin targets multiple essential cell processes, including DNA replication and repair

To further elucidate the effect of saccharin on *E. coli* and gain a greater insight into the cause of the aberrant morphologies and cell division phenotypes, we performed a differential RNA sequencing (dRNA-seq) experiment comparing cultures exposed to 1.4% saccharin for 1 hour to a mock treatment control. This analysis identified a total of 724 genes that were differentially regulated (Supplementary Table S1), with 419 significantly downregulated greater that |LogFC| >1 and 305 genes significantly downregulated greater that |LogFC| >1. Within the dRNA-seq data, we identified several membrane-associated genes being differentially regulated after saccharin exposure, which is concomitant with our observed effect on cell morphology. Specifically, the most downregulated gene was the outer membrane porin OmpF, while pathways associated with

O-antigen LPS biosynthesis and peptidoglycan biosynthesis were significantly upregulated. This suggests a cellular response to cell envelope damage triggered by saccharin. Intriguingly, a KEGG pathway analysis showed that β-lactam resistance mechanisms were significantly upregulated (Supplementary Table S2). Indeed, the impact on cellular morphology of saccharin is remarkably similar to that of peptidoglycan-targeting β-lactam antibiotics, with cellular filamentation and bulges forming on the cell membrane followed by cell lysis (Yao *et al.,* 2012). This suggests the cell may be responding to saccharin in a similar manner as to how it responds to antibiotic exposure, in particular to the β-lactam class.

A striking observation revealed by the KEGG pathway analysis was that amongst the most significantly upregulated pathways were the DNA replication and mismatch repair systems. This suggests a previously unreported effect of saccharin on bacterial genome dynamics. For this reason, we sought to explore the effect of saccharin on *E. coli* by monitoring the DNA replication dynamics in the cell during exposure to this artificial sweetener.

Saccharin interferes with DNA replication dynamics

The primary source of DNA replication under physiological conditions is chromosomal replication from the origin of replication (*ori*) region, forming two replisomes that move through the chromosome in opposite directions until reaching the termination region (*ter*). To explore a potential impact on *ori*-initiated DNA synthesis following 1.4% saccharin exposure, we treated an *E. coli* strain in which the *ori* and *ter* regions of the chromosome can be tracked by fluorescent repressor-operator systems (FROS; Figure 2A). Figure 2B shows the distribution of *ori* and *ter* foci corresponding to each documented cell after 60 min treatment. In the control, in which cells are able to start up to three rounds of chromosomal replication before division in 60 min, we can observe the expected 2-4 *ori* foci and the *ter* foci lagging one step behind in the duplication

progression (1-2 foci). However, after 1.4% saccharin treatment, there is an amplification of both *ori* and *ter* foci, with the distribution of *ori* foci shifting towards 8-16 counts and beyond. The *ter* foci follow a similar trend but lagging behind in the duplication progression, as would be expected.

One possible explanation for this would be that the lack of cell division caused by saccharin may lead to an accumulation of replicating chromosomes in the filamented cells, in the same replicative state as though they had successfully accomplished division. The control condition shows that *ori* and *ter* account for 2-4 and 1-2, respectively. Cell division in *E. coli* occurs every 19-20 minutes. Within our experimental window, we would expect a maximum of 3 division events, but given that this is an asynchronous growing culture, we would expect the majority of cells to have undergone 2 division events. This would lead to the majority of cells accumulating 8-16 and 4-8 *ori* and *ter* foci, respectively, which aligns approximately with the distribution observed for the saccharin treatment. This suggests that *ori*-initiated chromosomal replication is not significantly impacted by saccharin, but that multiple chromosomes undergoing replication accumulate in a saccharin-induced filamented cell. Nevertheless, *ori*-initiated replication is not the only possible source of DNA synthesis in the cell that could be potentially impacted by saccharin.

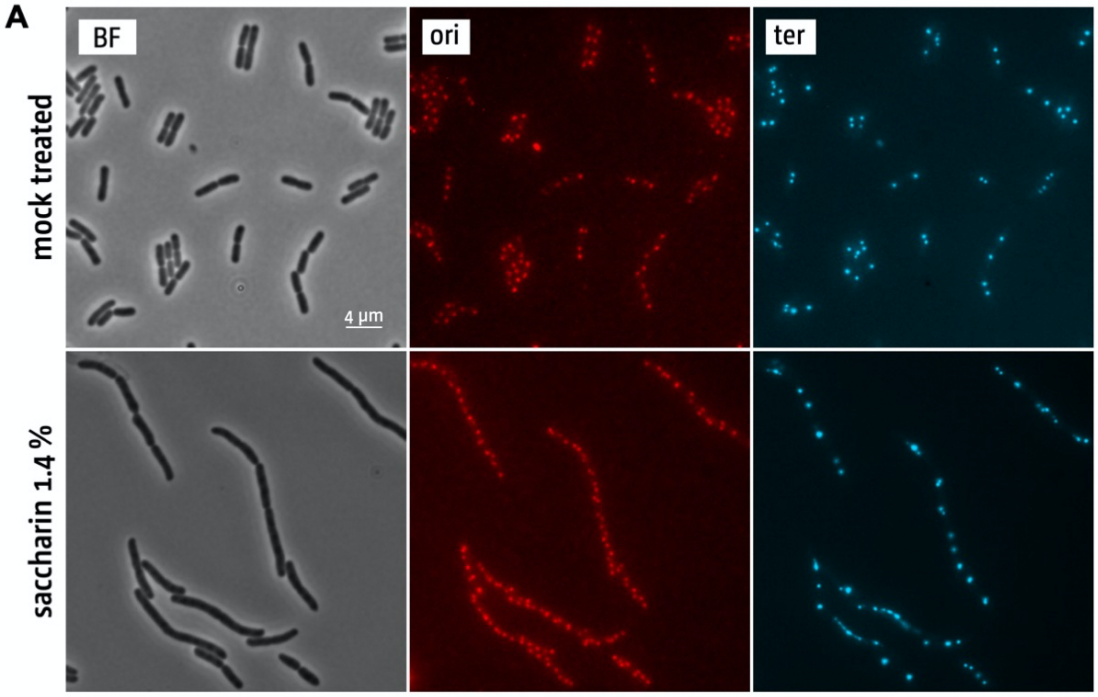
A
BF
ori
ter
mock treated
saccharin 1.4 %
4 µm

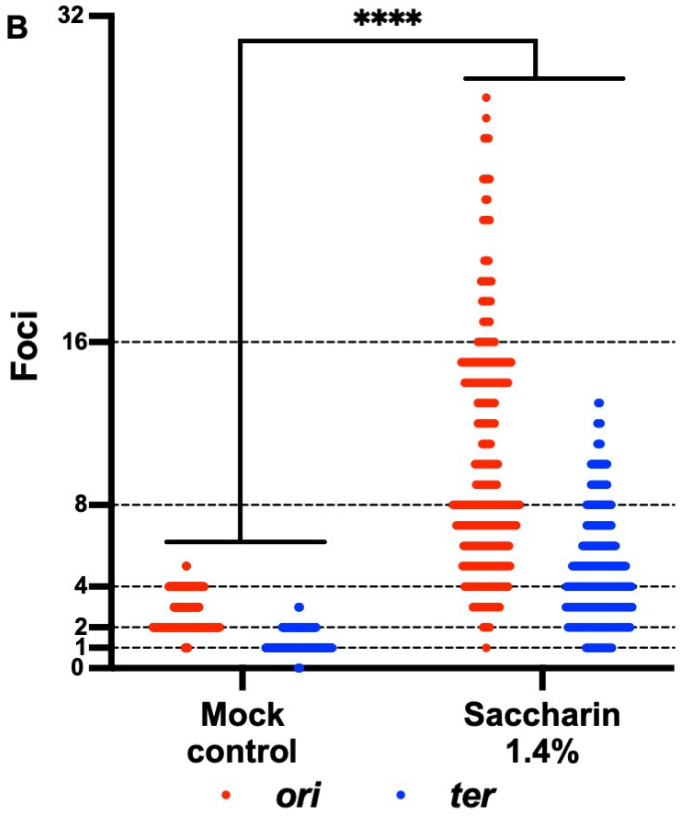
B
****
32
16
8
4
2
1
0
Foci
Mock control
Saccharin 1.4%
ori
ter

Figure 2: *ori*-dependent replication dynamics in living cells following treatment with saccharin. A) The origin and terminus area of the chromosome can be visualised via fluorescent repressor-operator arrays (FROS). The origin region is shown in red, whereas the terminus region is shown in cyan. Cells were grown to early exponential growth phase in LB broth (Miller). Untreated cells show foci numbers typically observed with growth conditions that allow overlapping rounds of DNA synthesis, resulting typically in 2-4 *ori* foci and 1–2 *ter* foci per cell. B) Treatment with saccharin results in a significant increase in the number of both origin and terminus foci, indicating amplification of both the origin and terminus areas in treated cells. Foci numbers were quantified across three independent biological replicates with at least three random frames with greater than 50 cells visible selected from each replicate and foci numbers pooled. Dashed lines indicate the theoretically possible foci numbers expected from a normal duplication progression. One representative image is shown in panel A. Results shown in panel B were analysed by Mann-Whitney test between treated and control samples for *ori* and *ter* foci. Significance is indicated as **** = $p \leq 0.0001$.

To test if saccharin may affect DNA synthesis initiated at sites other than the *ori*, we first tested an*E. coli* coding a thermosensitive version of the chromosomal *ori*-dependent replication initiation protein DnaA (*dnaA*(ts)) and carrying a fluorescent DnaN reporter, which allows direct visualisation of the replisomes. In this strain, chromosomal replication ceases upon a shift to 42 °C (Rudolph *et al.,* 2009) . In mock treated cells, we could observe a shift of DnaN foci to lower amounts at this restrictive temperature compared to 30 °C as expected. However, cells treated with 1.4% saccharin showed an increase in DnaN foci numbers both at 30 °C and 42 °C compared to the mock treated cells, which suggests that saccharin may be directly or indirectly triggering DNA synthesis away from the *ori* (Supplementary Figure S2). . To explore this further, we tested an *E. coli* strain over-expressing an eYFP-labelled Cas1-Cas2 complex (Cas1-LFP). It was recently shown that this protein complex localises into distinct foci where DNA is being actively

synthesised, allowing its use as a biomarker of active DNA synthesis (Killelea and Dimude *et al*., 2023). Using this reporter, we could see that a mock-treated population would be mostly represented by cells with 1-2 Cas1-LFP-Cas2 foci, with part of the population shifted towards 4 foci. However, the distribution of cells dramatically shifted towards a population with increased Cas1-LFP-Cas2 foci numbers (Figure 3A,B). A control Cas1[R84G] derivative, unable to bind DNA, did not show changes in foci numbers when treated with saccharin, highlighting the specificity of this effect (Supplementary Figure S3). Following a similar duplication progression as explained above, and again considering that filamented cells would have skipped a maximum of 3 divisions, with most cells having undergone 2 division within the time frame monitored, it would be expected that they would contain 8-16 foci should this phenomenon be a result of signal accumulation in non-dividing cells. However, the cell population distribution continues to trend toward 32 foci per cell. Increasing the concentration of saccharin from 1.4% to 2% further exacerbates this trend with a greater proportion of cells with more than 16 foci, suggesting a dose-dependent effect. To explore the specificity of this phenotype, we tested another artificial sweetener, ace-K, which has previously also been reported to induce filamentation (de Dios *et al.,* 2023). However, the ace-K treatment did not have a major impact on DNA replication dynamics, with the vast majority of cells having <8 foci, even at concentrations higher than those used for saccharin (Supplementary Figure S4). This confirms the active accumulation of a specific DNA substrate in saccharin-treated cells that is bound by Cas1-LFP-Cas2 complexes due to saccharin.

Although we acknowledge that the lack of cell division likely has a contribution to the increase in the ploidy of cells upon saccharin exposure, the shift in the distribution to DNA synthesis foci numbers beyond those expected by a physiological duplication progression coupled to cell division

made us hypothesise that repairing DNA damage may be responsible for the increased DNA synthesis observed in our microscopy and transcriptomic data.

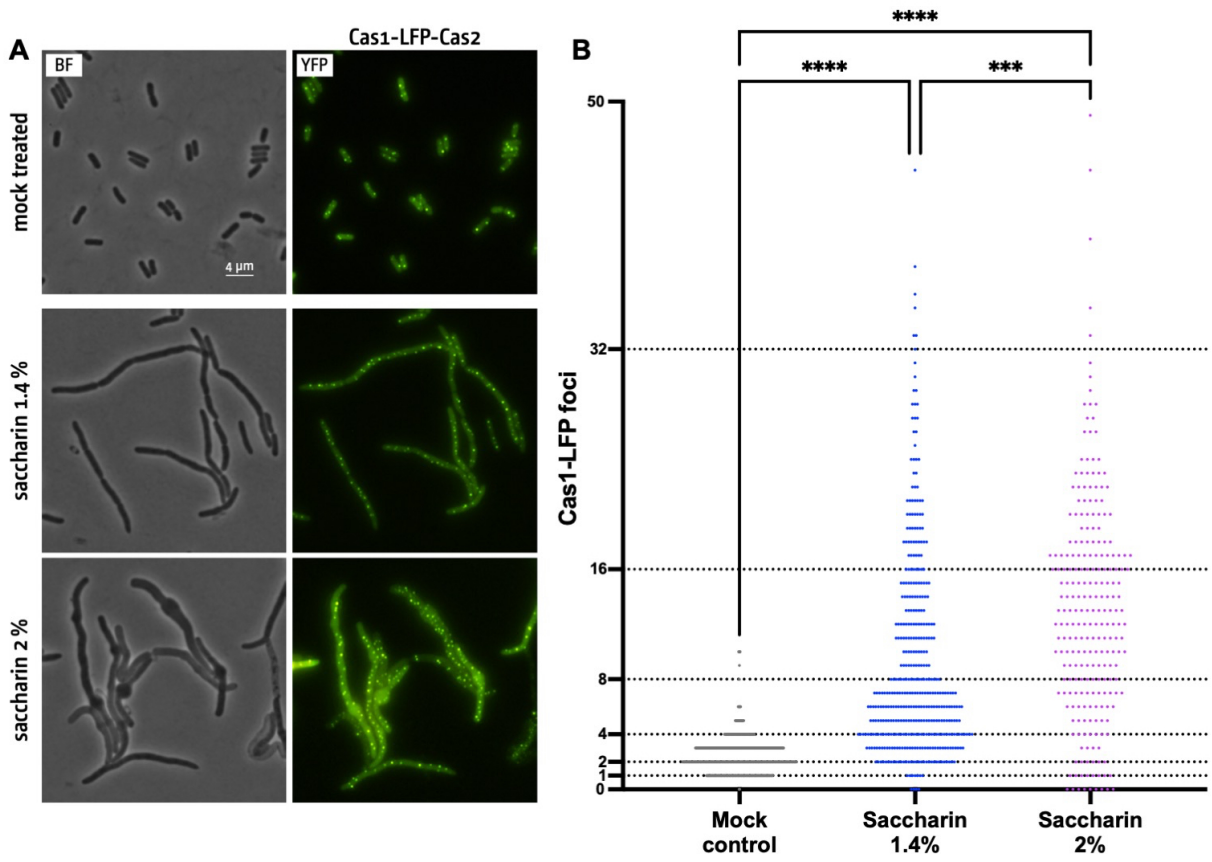

Figure 3: Cas1-LFP foci behaviour alters dramatically following treatment with saccharin. A) *E. coli* MG1655 cells were grown to early exponential growth phase in LB broth (Miller) and expression of Cas1-linker-eYFP (called Cas1-LFP for simplicity) and Cas2 induced by the addition of 0.1% arabinose for 60 min before visualization. As shown recently (Killelea and Dimude *et al*., 2023), active DNA replication results in robust focus formation of Cas1-LFP and Cas2, resulting in the majority of cells showing between 1 and 4 Cas1-LFP-Cas2 foci per cell. Following treatment with saccharin, this pattern is dramatically altered, with cells showing significantly higher foci numbers. The strain used was JD1708. **B)** Quantification of Cas1-LFP-Cas2 following saccharin treatment. Shown are foci distributions highlighting the concentration-dependent increase of foci following treatment. Foci numbers were quantified across

three independent biological replicates with at least three random frames with greater than 50 cells visible selected from each replicate and foci numbers pooled. Dashed lines indicate the theoretically possible foci numbers expected from a normal duplication progression. One representative image is shown in panel A. Results shown in panel B were analysed by Kruskal-Wallis test with Dunn's correction. Significance is indicated as *** = $p \leq 0.001$, **** = $p \leq 0.0001$.

Does saccharin trigger DNA repair?

At this point, we have shown multiple, independent lines of evidence (dRNA-Seq, *dnaA* (ts) and concentration dependent effects, Supplementary Table S2, Supplementary Figure S2 and Figure 3) to suggest that saccharin may be triggering DNA repair pathways. It was shown previously that saccharin induces DNA strand breaks in mouse bone marrow cells that can be visualised by the COMET assay (Bandyopadhyay *et* al., 2008). Damaged DNA ends are the substrate for a process called break-induced replication (BIR), a mechanism where the invasion of a processed DNA end into a homologous template can trigger DNA synthesis away from the origin (Kockler *et* al., 2021). This repair pathway requires the processing of DNA intermediates by the replication restart pathways, PriA/PriB, PriA/PriC and PriC, to load the replicative helicase DnaB (Anand *et al*., 2013; Windgassen *et* al., 2018; Michel and Sandler, 2017.). To distinguish between synthesis initiated at the *ori* and elsewhere within the chromosome to mediate repair after saccharin treatment, we quantified the number of replisomes per cell using the Cas1-LFP-Cas2 reporter in the wild type *E. coli* or in mutants in *priB* or *priC*. If DNA synthesis triggered by saccharin treatment is mostly induced at the origin, and not by DNA damage, the *priB* and *priC* mutations should have little or no effect on the accumulation of Cas1-LFP-Cas2 foci. Indeed, treating with 1.4% saccharin produced an increase in Cas1-LFP-Cas2 foci in the wild type as well in the Δ*priB* and Δ*priC* mutants (Figure 4A,B). However, the accumulation of foci in both mutants was

287 significantly lower than that observed for the wild type *E. coli*. This would indicate that the
288 accumulation of Cas1-LFP-Cas2 foci in response to saccharin exposure is at least partially
289 dependent on BIR pathways, which together with the previous literature may suggest that
290 saccharin produces DNA damage in this model, or at least that it triggers the BIR pathways.
291 Importantly Δ*priB* and Δ*priC* mutants exhibited the same cell filamentation response as the wild-
292 type upon saccharin exposure, therefore excluding the impact of inhibited cell division on overall
293 foci counts. The impact of saccharin on DNA replication dynamics appears to be non-lethal
294 however, as typically we did not observe cell lysis prior to 60 minutes (Figure 1AB, Supplementary
295 Video S1, Supplementary Video S2) but routinely observed impacts on DNA replication
296 dynamics, confirming cell viability, within this timeframe. This would suggest that bulge-mediated
297 cell lysis is the primary mechanism through which saccharin mediates cell death. It would be
298 intriguing to investigate the longer-term consequences of these impacts on DNA synthesis and
299 replication, but due to the lysis of the cells this is not possible within the current experimental set-
300 up.

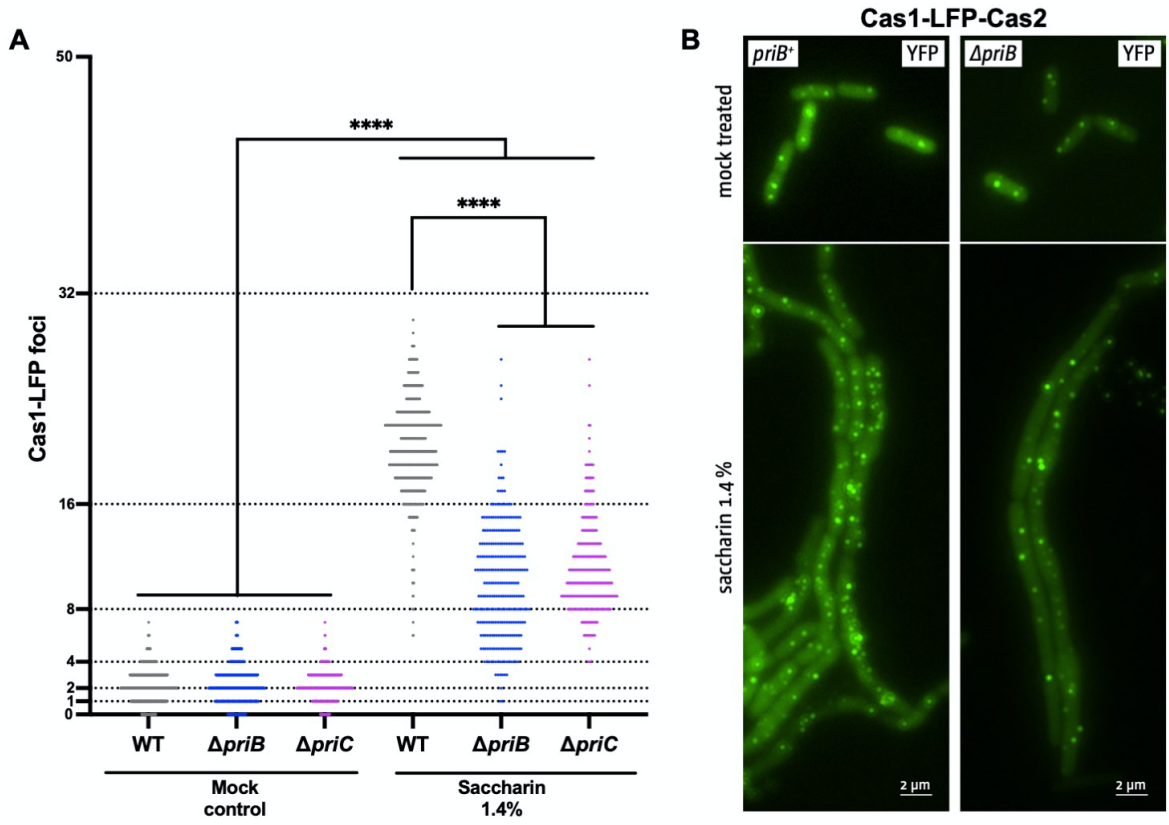

Figure 4. Cas1-LFP foci formation in saccharin-treated cells is significantly reduced in cells lacking the replication restart proteins PriB and PriC. A) *E. coli* MG1655 cells with and without functional PriB or PriC restart proteins were grown to early exponential growth phase in LB broth (Miller) and either treated with saccharin as indicated, or mock treated for 60 min. Simultaneously, expression of Cas1-linker-eYFP (called Cas1-LFP for simplicity) and Cas2 was induced by the addition of 0.1% arabinose. While in untreated cells the absence of PriB or PriC did not result in a reduction in foci numbers, the filamented cells following saccharine treatment do show foci amplification in the absence of either PriB or PriC, but to a significantly lesser extent than in wild type cells. B) A representative example comparative visualisation of the effect of mutating a BIR pathway (only *priB* in this case, as the Δ*priC* mutant showed a similar phenotype) is shown. Foci numbers were quantified across three independent biological replicates with at least three random frames with greater than 50 cells visible selected from each replicate and foci numbers pooled. Dashed lines indicate the theoretically possible foci numbers expected from a normal duplication

progression. One representative image is shown in panel B. Results shown in panel A were analysed by Kruskal-Wallis test with Dunn's correction. Significance is indicated as **** = p ≤0.0001, ns = non-significant.

Saccharin inhibits growth of clinically relevant pathogens.

To this point, saccharin has shown an inhibitory activity on an *E. coli* lab model, directly impacting cell division and morphology, as well as DNA replication dynamics. Furthermore, our transcriptomics analysis showed that *E. coli* might be responding to saccharin by activating similar pathways to those triggered by β-lactam antibiotics. Indeed, our group and others previously showed that saccharin can inhibit the growth of clinically relevant pathogens, such as *A. baumannii* and *P. aeruginosa* (Sunderhauf et al., 2020, Yu et al., 2022, Yu and Guo, 2022, de Dios *et al*., 2023). Altogether, these evidence for the potential of saccharin to inhibit bacterial growth by impacting different pathways prompted us to comprehensively test its antimicrobial effect on clinically relevant pathogenic isolates.

To uncover the full spectrum of saccharin antimicrobial activity, as well as the levels of inhibition, we applied a range of concentrations to a panel of high priority pathogen clinical isolates, including MDR *E. coli*, *S. aureus*, *K. pneumoniae*, *A. baumannii* and *P. aeruginosa.* Saccharin was capable of inhibiting growth of all the strains tested in a dose-dependent manner (Figure 5). However, the relative levels of this inhibition varied between pathogens. *E. coli, S. aureus*, *K. pneumoniae* and *A. baumannii* showed a major reduction in growth (>70%) at a concentration of 2%, whereas *P. aeruginosa* required a concentration of 6 % to achieve similar levels of growth inhibition (77% reduction in growth). As for the different pathogens tested (except for *P. aeruginosa*) a sudden drop in viability occurred within the 1-2% saccharin interval, we calculated IC50 values

337 (concentration producing a 50% of total inhibition) in that range (Supplementary Figure S1). As
338 result, the IC50 ranged from 1.2-1.5%, except in the case of *P. aeruginosa*, for which the IC50
339 was 2.5%. These results indicate that saccharin is effective at inhibiting the growth of both Gram-
340 negative and Gram-positive pathogens. Furthermore, the varying levels of growth inhibition in a
341 species-specific manner may explain the variable effects of saccharin reported previously on the
342 microbiome (Suez *et al.,* 2014). In addition, this would support the hypothesis that saccharin could
343 alter the populational balance of the microbiome, rather than impacting the fitness of all the
344 members of this ecosystem alike.

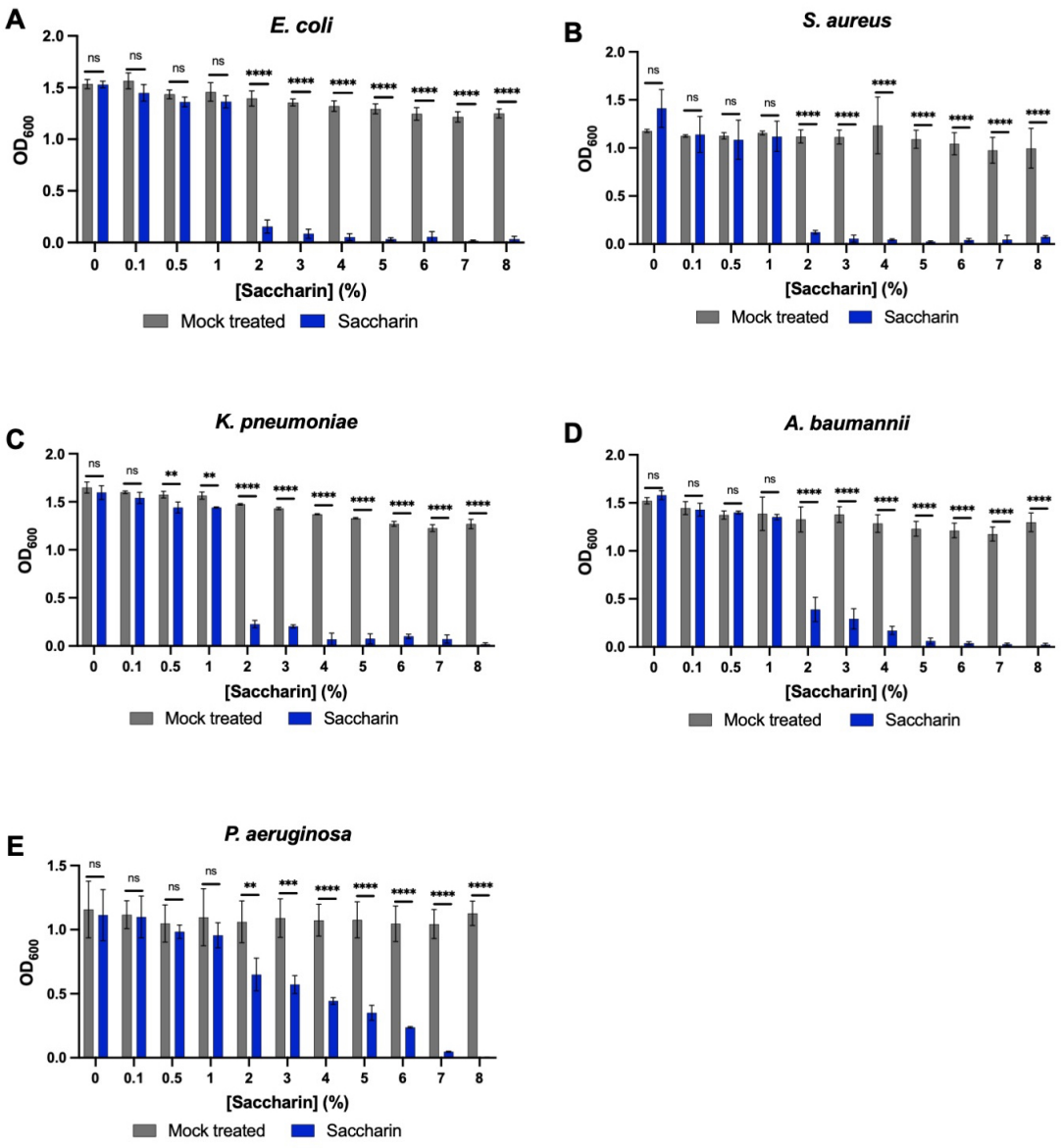

Figure 5. Saccharin displays dose-dependent growth inhibitory effects against both Gram-positive and Gram-negative pathogens. Growth inhibition of *E. coli* (**A**), *S. aureus* (**B**), *K. pneumoniae* (**C**), *A. baumannii* (**D**) and *P. aeruginosa* (**E**) at a range of saccharin concentrations (0, 0.1, 0.5, 1, 2, 3, 4, 5, 6, 7, 8 %). Inhibition was shown to be dose-dependent across all tested pathogens. For all assays, experiments were performed in biological triplicate, each performed in technical triplicate. Statistical analysis consisted of two-way ANOVA with Sidak's correction between the saccharin treated samples and the water controls,

for all panels. Average values ± S. D. are represented. Significance is indicated as ** = p ≤0.01, *** = p ≤0.001, **** = p ≤0.0001, ns = non-significant.

Saccharin disrupts biofilm formation and motility

Biofilm formation during infection represents a major healthcare issue, as this bacterial lifestyle allows pathogens to remain recalcitrant to antibiotic treatments and the rigors of the host immune system (Kumar *et al*., 2017, Jamal *et al*., 2018, Roilides *et al*., 2015). To explore if saccharin has anti-biofilm properties, we assessed its ability to inhibit *de novo* biofilm formation in two particularly notorious biofilm forming pathogens, *A. baumannii* and *P. aeruginosa* (Mulcahy *et al*., 2014, Maslova *et al*., 2021, Harding *et al*., 2018). Their levels of biofilm formation supported a better resolution to test a possible anti-biofilm activity of saccharin, compared to the negligible biofilm formation observed for *E. coli* (even without treatment) in the conditions tested (Supplementary Figure S5). We observed that saccharin could indeed inhibit this behaviour, showing a reduction of 97.5% for *A. baumannii* and 91.7% for *P. aeruginosa* at a 2% concentration (Figure 6A,B). This greater reduction in biofilm formation than in bacterial growth suggests that this sweetener may have anti-biofilm properties. This is specifically supported by the anti-biofilm profile of saccharin on *P. aeruginosa* (Fig. 6B), where the steadier decrease in viability over saccharin concentrations (Fig. 5E) allows a better distinction between antimicrobial and anti-biofilm effect.

Disrupting established biofilms is a key clinical challenge, particularly with respect to wound and indwelling device associated infections (Maslova *et al*., 2021, Pelling *et al*., 2019). To evaluate if saccharin could disrupt a mature biofilm, we conducted biofilm disruption assays. As previously

observed for biofilm inhibition, saccharin could disrupt mature biofilms of *A. baumannii* and *P. aeruginosa* to different levels depending on the species (Figure 6C). In the case of *A. baumannii*, a treatment with 8% saccharin resulted in a reduction of a 30.2% in the biofilm biomass, whereas for *P. aeruginosa,* the treatment achieved a striking 81.2% reduction in the biofilm biomass compared to the vehicle control. Together, this positions saccharin as a potential anti-biofilm agent, not only to prevent biofilm formation, but to disrupt established biofilms such as those associated with chronic infections.

Twitching motility is an important virulence behaviour for many *A. baumannii* strains, including AB5075. It is mediated by type IV pili, which play a dual role in this type of motility as well as in adhesion (Ronish *et al*., 2019, Ellison *et al*., 2022). We previously demonstrated that sub-inhibitory concentrations of the artificial sweetener ace-K could abolish twitching motility in AB5075 (de Dios *et al*., 2023). For this reason, we tested if this effect was replicated by a range of saccharin concentrations. As a result, we obtained a dose-dependent inhibitory effect of saccharin on the twitching motility of AB5075 (Figure 6D). Remarkably, this inhibition occurred at sub-inhibitory concentrations of saccharin (1% and below), showing the anti-virulence potential of this sweetener against an MDR strain of the critical priority pathogen *A. baumannii*.

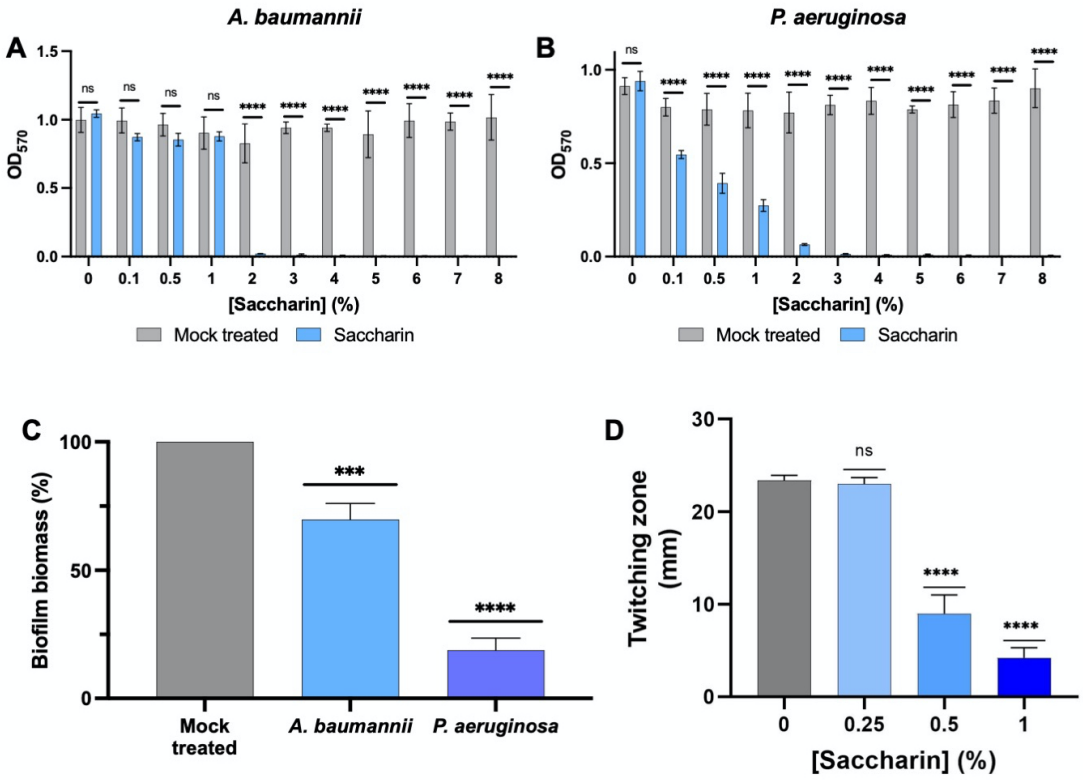

Figure 6. Saccharin inhibits biofilm formation and twitching motility in a dose-dependent manner and can disrupt preformed biofilms. Inhibition of *de novo* biofilm formation of *A. baumannii* (**A**) and *P. aeruginosa* (**B**) at a range of saccharin concentrations (0, 0.1, 0.5, 1, 2, 3, 4, 5, 6, 7, 8 %). Inhibition showed to be dose-dependent across the range of concentrations. The ability of an 8% saccharin solution to disrupt preformed *A. baumannii* and *P. aeruginosa* biofilms was also assessed (**C**). For both pathogens, the treatment produced a 30.2% and an 81.2% reduction in biofilm biomass, respectively. The percentage of biofilm biomass was calculated as the biofilm formation measurement for the treated samples with respect to the untreated control for each species. (**D**) Twitching motility assays using *A. baumannii* AB5075 over a range of concentrations of saccharin (0-1%). Biofilm assays were performed in biological triplicate, each performed in technical triplicate. Twitching assays were performed as five biological replicates. Statistical analysis consisted of two-way ANOVA with Sidak's correction between the saccharin treated samples and the water controls for panels A and B, and one-way ANOVA with Dunnett's correction for panels C and D. Average values ± S. D. are represented. Significance is indicated as * = $p \leq 0.05$, ** = $p \leq 0.01$, *** = $p \leq 0.001$, **** = $p \leq 0.0001$, ns = non-significant.

404

405 **Saccharin can inhibit and disrupt polymicrobial biofilms.**

406 Within an infection context, polymicrobial communities of multiple pathogens are more frequently
407 observed than single-species biofilms (Gabrilska *et al*., 2015, Anju *et al*., 2022, Kulshrestha *et al*.,
408 2022, Maslova *et al*., 2021). Within these communities, cooperative interactions can take place,
409 with different species protecting the whole community from insults, such as antibiotics, via the
410 production of community resources. As a result, these polymicrobial biofilms remain much more
411 recalcitrant to treatment and are commonly associated with chronic wounds (Kirketerp-Møller *et*
412 *al*., 2020, Alvarado-Gomez *et al*., 2018, Maslova *et al*., 2021). As the three most common
413 pathogens usually co-isolated from wounds are *P. aeruginosa, A. baumannii* and *S. aureus,* we
414 tested the ability of saccharin to inhibit and disrupt a polymicrobial biofilm involving these three
415 species (Dent *et al*., 2010, Dowd *et al*., 2008, Fazli *et al*., 2009). To confirm that a polymicrobial
416 biofilm was formed, we grew a biofilm for 24 h starting with equal OD_{600} amounts of each of the
417 three species, disrupted it and cultured the resulting cell suspension in selective media for each
418 pathogen. Despite expected variations in the species-to-species proportions by the end of the
419 experiment, we could consistently recover all three pathogens from the biofilm, hence confirming
420 its polymicrobial nature (Supplementary Figure S6). We then tested the effect of saccharin on the
421 inhibition of *de novo* biofilm formation, observing that the presence of 1% saccharin resulted in a
422 27.9% reduction in biofilm formation (Figure 7A). With respect to disruption of an established
423 polymicrobial biofilm, the treatment with an 8% saccharin solution resulted in a 54.6% reduction
424 of the biofilm biomass (Figure 7B). The capacity to overcome this notoriously recalcitrant mode
425 of multispecies growth highlights the therapeutic potential of saccharin.

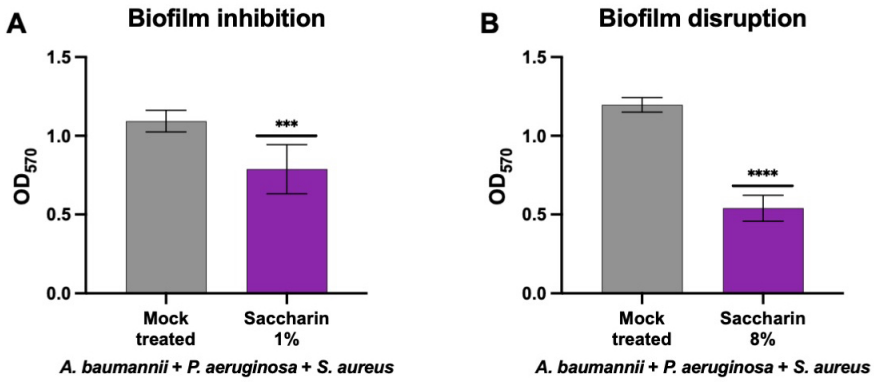

Figure 7: Saccharin inhibits polymicrobial biofilm formation and disrupts polymicrobial biofilms: **A**) Inhibition of *de novo* biofilm formation in mixed cultures containing a 1:1:1 ratio of *P. aeruginosa, A. baumannii* and *S. aureus* in LB media supplemented with either 1% saccharin or a vehicle control and incubated at 37˚C. The treatment produced a significant reduction in the polymicrobial biofilm formation. **B)** Disruption of preformed polymicrobial biofilms from mixed cultures containing a 1:1:1 ratio of *P. aeruginosa, A. baumannii* and *S. aureus* in LB media after treating with 8% saccharin or a vehicle control for 24 h. The treatment produced a significant reduction in the polymicrobial biofilm biomass. Assays were carried out in biological triplicate. Statistical analysis consisted of Student's t-test between the saccharin treated samples and controls. Average values ± S. D. are represented. Significance is indicated as *** = $p \leq 0.001$, **** = $p \leq 0.0001$.

Saccharin produces pleiotropic gene expression changes in MDR *A. baumannii*

Despite having obtained conclusive mechanistic data showing that the antimicrobial effect of saccharin involves alterations of the genome dynamics and DNA damage using a lab *E. coli* strain, this model would not be representative of a clinically relevant scenario. For this reason, and given the urgent need for novel therapeutic approaches against MDR *A. baumannii*, we decided to conduct a dRNA-seq experiment using *A. baumannii* AB5075 as a model. We compared the presence of a sub-inhibitory concentration of saccharin (1%) to a mock treatment. This sub-

444 inhibitory concentration was chosen to give a greater insight into the antivirulence effects mediated
445 at these sub-inhibitory concentrations. In these conditions, a total of 380 genes were more than 1-
446 log differentially regulated, with 165 upregulated and 215 downregulated (Figure 8A,
447 Supplementary Table S3). To assess if there was any specific functional group of genes directly
448 affected by the presence of saccharin, we performed a gene set enrichment analysis (GSEA) among
449 the genes that were either up- or downregulated. As a result, we obtained that the only functional
450 group significantly enriched among the downregulated genes (Supplementary Table S4) was that
451 encompassing genes related to pili and fimbriae biogenesis as per their annotation (ABUW_0648,
452 ABUW_1632, ABUW_1633, ABUW_2052, ABUW_2053 and ABUW_2310) (Gallagher *et al*.,
453 2015). These genes are well known for their role in adhesion and biofilm formation in *A.*
454 *baumannii* (Colquhoun *et al*., 2020). In addition to these, we could also find three genes belonging
455 to the Type IV pili, including *pilN* and *pilO* (ABUW_0291 and ABUW_0292, respectively), which
456 are part of the inner membrane complex, and the major pilin subunit *pilA* (ABUW_0304). This
457 validates our previous findings showing the inhibitory effect of saccharin on the twitching motility
458 of AB5075 (Figure 6D). Furthermore, this downregulation, as well as that of the biofilm-related
459 gene *blp2* (ABUW_1120), was coherent with the decreased biofilm formation in the presence of
460 saccharin shown above (de Gregorio *et al*., 2015). With respect to the upregulated genes, no
461 functional enrichment was observed.

462 Other examples of gene groups that consistently appeared among the differentially regulated genes
463 were either involved in iron homeostasis or encoding iron-bound proteins (ABUW_1348,
464 ABUW_1776, ABUW_2186, ABUW_2458, ABUW_2546, ABUW_2953, ABUW_3843,
465 ABUW_3484, ABUW_3806) and multiple genes linked to sulphur metabolism (*cysN, cysT, cysW,*
466 *sfnG, tauA, tauC, tauD,* ABUW_1021, ABUW_1941, ABUW_2169, ABUW_2335,

467 ABUW_2336, ABUW_3853) according to their annotation (Gallagher *et al*., 2015). This
468 suggested that iron and/or sulphate homeostasis or acquisition pathways may be disturbed in the
469 presence of saccharin. However, supplementing with neither ferric iron nor sulphate could
470 alleviate the growth inhibition produced by saccharin (Supplementary Figure S7, Supplementary
471 Figure S8).

472 In addition to the previously mentioned gene expression alterations, a frequent signature we could
473 observe among the differentially regulated genes was the association to the cell envelope. At least
474 67 differentially regulated genes were related to this structure (Supplementary Table S5) either
475 directly as per their annotated gene description or being functionally associated to it (for example,
476 being involved in transport, secretion or biofilm formation) (Gallagher *et al*., 2015). This supported
477 our previous data that membrane stability is compromised after saccharin treatment, thus
478 producing an impact on fitness in combination with the disruption of DNA replication dynamics
479 (Mitchell *et al*., 2019). As divalent cations are known to stabilise the cell envelope of Gram-
480 negative bacteria by bridging the lipopolysaccharide molecules in the outer membrane, we further
481 tested this hypothesis by supplementing the media with Ca^{2+} and Mg^{2+}(Clifton *et al*., 2015). This
482 resulted in a partial relief of the growth inhibition (Figure 8B). Although this rescue effect seemed
483 modest with respect to the total inhibitory effect exerted by saccharin, this result may support that
484 this artificial sweetener disrupts the integrity of the cell envelope.

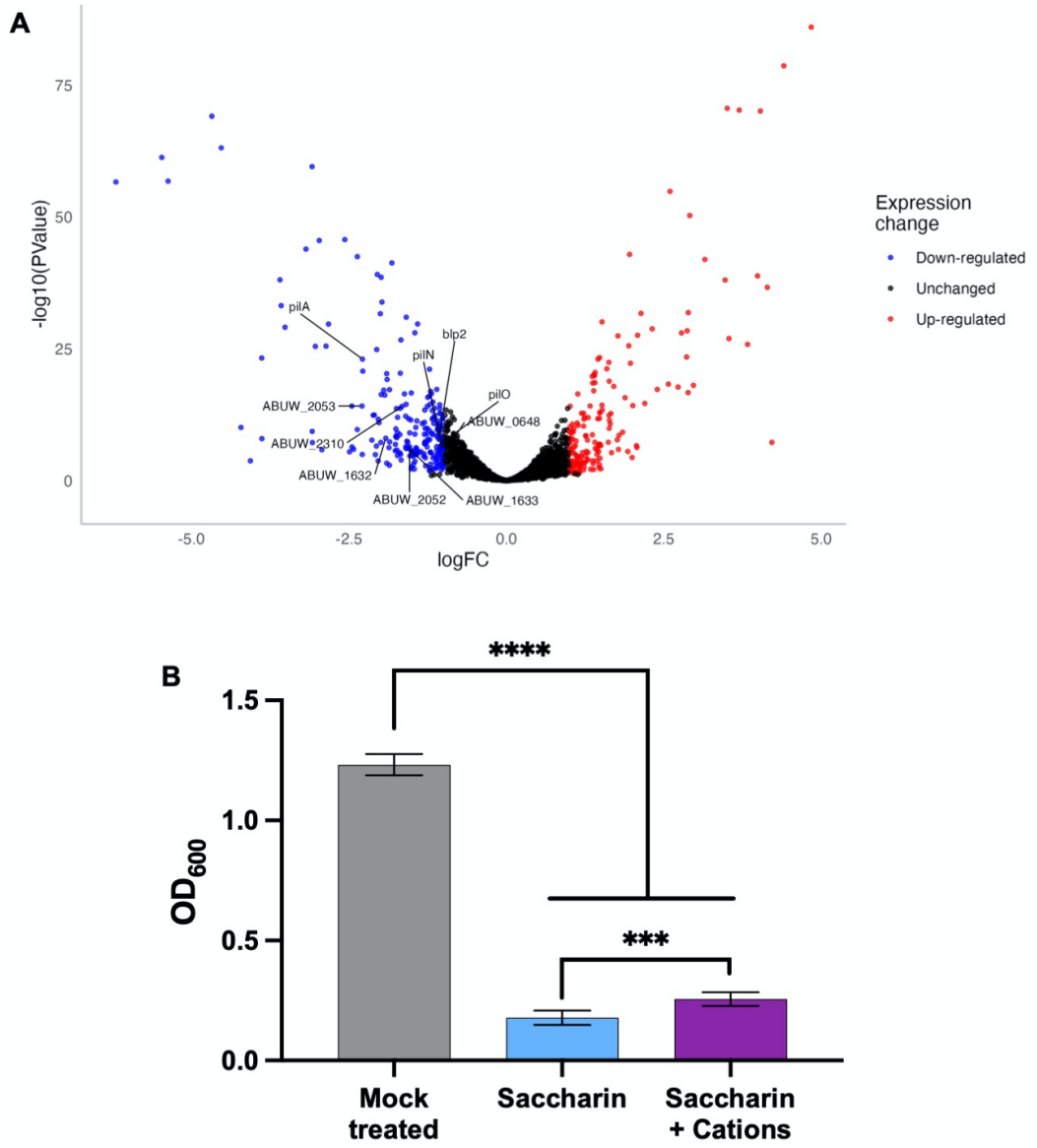

485 **Figure 8**: **Saccharin produces an impact on different functional groups of genes in MDR *A. baumannii***
486 ***AB5075*: A**) Volcano plot representing dRNA-seq results comparing cells treated with 1% saccharin to a
487 mock treatment. According to the dRNA-seq results, 165 genes were upregulated (red) and 215 were
488 downregulated (blue). In the interest of visualisation, ABUW_0607 was removed from the volcano plot (a
489 plot version including this gene is shown in Supplementary Figure S9). **B**) The addition of cations (2 mM
490 $CaCl_2$ and 1 mM $MgSO_4$) can partially rescue the growth inhibitory effect of saccharin. Data represents the
491 mean of five biological replicates for motility and three biological replicates for cation supplementation ±

S.D. Analysis was done by one-way ANOVA with Tukey's correction to compare all conditions (*** p = <0.001, **** p = <0.0001, ns = non-significant).

Saccharin increases antibiotic transition across the cell envelope overcoming native resistance mechanisms

The damage to the membrane induced by saccharin exposure suggests that it could perturb the transition of molecules across the cell envelope, potentially impacting antibiotic uptake, and thus, susceptibility. To test this, we used MDR *A. baumannii* AB5075. Importantly for this pathogen, the low permeability of its cell envelope acts as an intrinsic antibiotic resistance mechanism (McCarthy *et al*., 2021). To first confirm that saccharin does induce an altered membrane morphology in *A. baumannii*, we used time lapse microscopy on cells exposed to 1.4% or 2% saccharin. The treatment induced a loss of cell morphology with cells ballooning rather than filamenting as was observed with *E. coli* cells (Figure 1A), characteristic membrane bulges were also visible (Figure 9A, Supplementary Video 3, Supplementary Video 4) suggesting that the membrane damaging effects of saccharin are consistent across species. Indeed, epifluorescence microscopy images of AB5075 cultures treated with a sub-inhibitory concentration of saccharin (1%) showed an increased permeability to DAPI than an untreated control (Supplementary Figure S10). This suggested that alterations in the *A. baumannii* envelope permeability induced by saccharin may increase the access of antibiotic to the cytosol. To further explore this, we tracked the uptake of multiple fluorescently labelled antibiotics after treating with a range of saccharin concentrations (0.5%-1.5%) using a flow cytometry approach. The antibiotics selected were the penicillin fluorescent derivative Bocillin and a vancomycin-BODIPY^{TM} FL conjugate (both penicillin and vancomycin inhibit peptidoglycan biogenesis by different mechanisms). We also

wanted to assess if the transition of a non-cell envelope targeting antibiotic across the cell envelope was impacted by saccharin. To this end we generated a bespoke neomycin probe (neomycin inhibits the ribosomal function) by conjugating it with Cy5, in analogy to a previously reported neomycin probe (Sabeti Azad *et al*., 2020). The various mechanisms of action of the selected fluorescent antibiotics would ensure that signal variations would depend on envelope permeability and not target availability or their physicochemical properties. Figure 9B shows the effect of 1.5% saccharin on cell morphology and antibiotic accumulation in *A. baumannii*, with both phenotypes being dose-dependent (Supplementary Figure S11). We could observe an increase in cell size, shifting from a 14.5-15.8% in oversized cell population with respect to total cells for all probes tested to 53.1%, 64.5% and 52.5% for Bocillin, Vancomycin-BODIPY^{TM} FL and Neomycin-Cy5, respectively. These similar results suggest that changes in cell morphology are due to the saccharin treatment and independent of the probe, and confirms the aberrant cell morphology induction by saccharin observed in our time lapse experiments (Figure 9A). On the other hand, we observed an increase in the populations labelled with the different probes, with shifts from 17.8% to 85.7%, 15.8% to 86.9% and 1.2% to 33.7% for Bocillin, Vancomycin-BODIPY^{TM} FL and Neomycin-Cy5, respectively. This indicates that, although the permeability of the *A. baumannii* envelope was uneven for the different probes, all of them showed an increased cell penetration after saccharin treatment.

As a next step, we investigated if the increased cell envelope permeability of *A. baumannii* to antibiotics after saccharin treatment would lead to an increased sensitivity to antibiotics. Specifically, *A. baumannii* strains resistant to the last-resort antibiotics carbapenems, such as AB5075, have been listed at the top of the WHO priority pathogen list. For this, we assessed the

538 minimum inhibitory concentration (MIC) of different carbapenems in the presence of 1% and 1.5%
539 saccharin on cation-adjusted Mueller-Hinton agar. The treatment resulted in a dramatic dose-
540 dependent decrease of the MIC, even dropping below the EUCAST breakpoint (2 mg/l for
541 doripenem and meropenem, 4 mg/l for imipenem) at a 1.5% concentration of saccharin (Figure
542 9C, Supplementary Figure S12). These findings support the potential of saccharin as an antibiotic
543 potentiator, prospectively opening new avenues to tackle recalcitrant MDR infections.

544

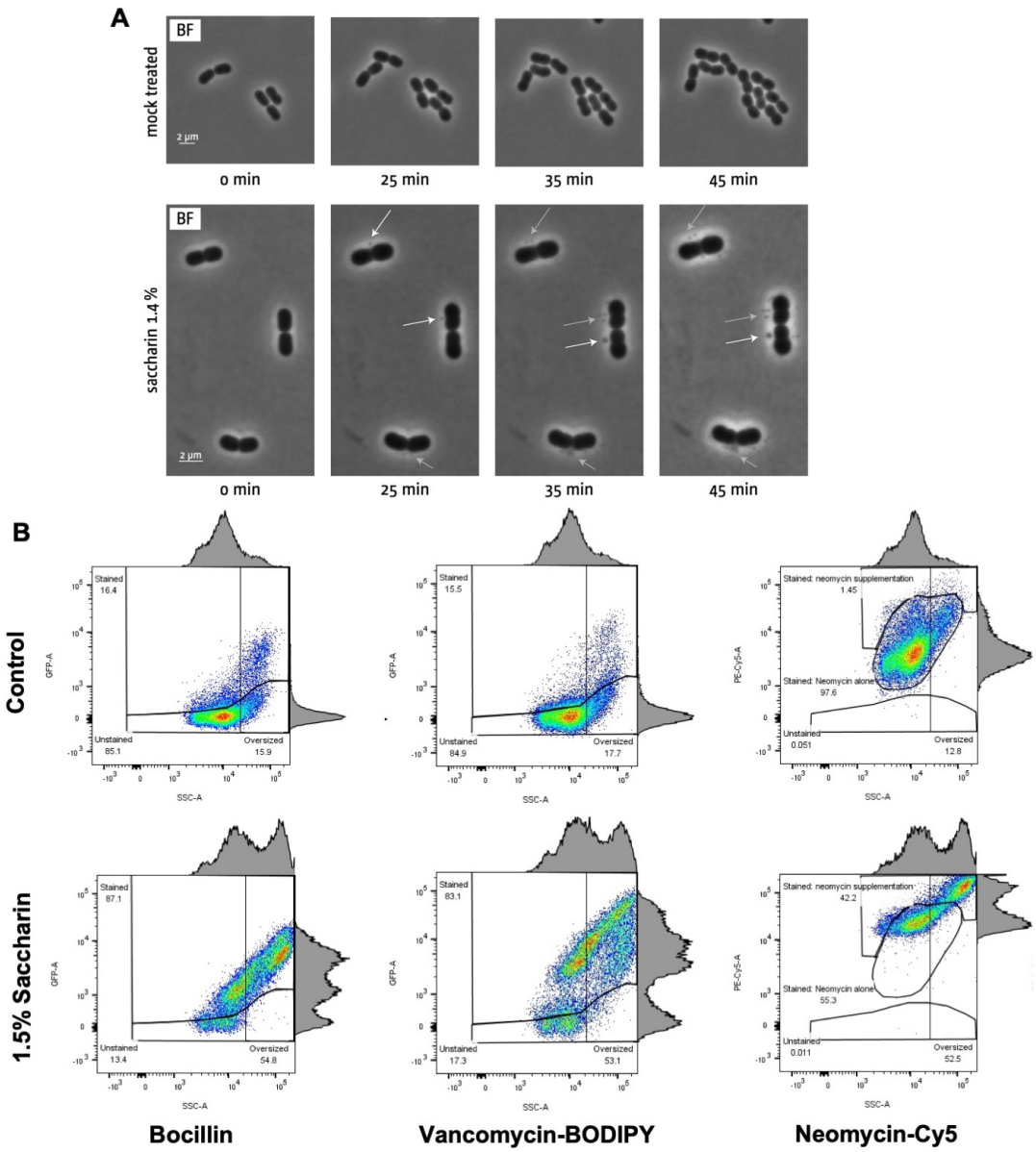
A
BF
mock treated
2 µm
0 min
25 min
35 min
45 min
BF
saccharin 1.4 %
2 µm
0 min
25 min
35 min
45 min
B
Control
1.5% Saccharin
Stained
16.4
Unstained
85.1
Oversized
15.9
Stained
15.5
Unstained
84.9
Oversized
17.7
Stained: neomycin supplementation
1.45
Stained: Neomycin alone
97.6
Unstained
0.051
Oversized
12.8
Stained
87.1
Unstained
13.4
Oversized
54.8
Stained
83.1
Unstained
17.3
Oversized
53.1
Stained: neomycin supplementation
42.2
Stained: Neomycin alone
55.3
Unstained
0.011
Oversized
52.5
GFP-A
PE-Cy5-A
SSC-A
Bocillin
Vancomycin-BODIPY
Neomycin-Cy5
C
MIC (mg/l)
40
30
20
10
0
****
ns
***
****
ns
****
****
ns
****
Doripenem
Imipenem
Meropenem
Control
Saccharin 1%
Saccharin 1.5%

545

Figure 9: Saccharin potentiates antibiotic activity against MDR *A. baumannii* AB5075 by increasing membrane permeability: A) Impact of saccharin on cellular growth and morphology of *A. baumannii* observed during time-lapse phase contrast imaging. *A. baumannii* AB AB5075 cells grown on LB medium without sweetener (0%) was used as a vehicle control, highlighting the normal growth pattern of *A. baumannii*. In the presence of 2% saccharin, the images shown highlight the formation of membrane bulges (white arrows), which eventually rupture, resulting in the spilling of cytoplasmic content into the surrounding area (grey arrows). An environmental chamber was used to maintain a constant temperature of 37 °C. Cells were imaged for 60 min. **B**) Exponential phase cells were treated with 1.5% saccharin or a mock treatment for 30 min. Then, they were incubated with 5 μM Bocillin, 5 μM Vancomycin-BODIPY^{TM} FL or 0.1 μM Neomycin-Cy5 for 30 min prior to flow cytometry. The results show a saccharin dose-dependent increase in fluorescent antibiotic labelling (Fluorescence signal, Y-axis) and cell size, which at this size range is best represented by the side scatter (SSC, X-axis). Cell size is represented in the X-axis (side scatter, SSCC) and fluorescence (fluorescent antibiotic labelling) in the Y-axis. Cell populations were gated according to cell size and unlabelled controls as shown in Supplementary Figure S11 and explained in the Methods section. The images presented are a representative example of 3 biological replicates. A representative example full range of saccharin concentrations tested (0-1.5%) and average labelling and cell size trends obtained from 3 biological replicates are shown in Supplementary Figure S11. **C**) We measured the MIC (Etest strips) for the carbapenems doripenem, imipenem and meropenem on Mueller-Hinton agar at sub-inhibitory concentrations of saccharin (1% and 1.5%) and a vehicle control. The results show a decrease of the MIC below the EUCAST breakpoint of each of the carbapenems at a concentration of 1.5% saccharin. The solid red line indicates the EUCAST breakpoint for doripenem and meropenem (2 mg/l); the dashed red line indicates the EUCAST breakpoint for imipenem (4 mg/l). In the control experiment, the imipenem MIC was above the detection limit of the Etest strip (32 mg/l). Data represents the mean of 3 biological replicates ± S.D. Analysis was performed by multiple-

comparison two-way ANOVA with Tukey's correction within the sample groups indicated for panel C (*** p = <0.001, **** p = <0.0001, ns = non-significant).

Saccharin-loaded hydrogels decrease bacterial burden in an *ex vivo* burn wound model

Given the emerging body of evidence that saccharin can inhibit bacterial growth and disrupt pathogenic behaviours such as biofilm formation, we next sought to explore its therapeutic potential. Wound healing is usually affected by the formation of biofilms, characteristic of chronic infection. Strikingly, there are relatively few topical antimicrobials in the drug development pipeline with anti-biofilm properties (WHO, 2022). In these situations, the preferred option is the application of the treatment by means of a hydrogel. This means of topical application outperforms other, such as soaked gauzes, due to the negative impact they may have on healing because of maceration and the lack of effective exudate management (Chamanga, 2015). For this reason, we formulated a saccharin-loaded tetraborate-PVA hydrogel. To firstly test its efficacy, we applied it for 1 h on early-stage *A. baumannii* AB5075 colony biofilms grown for 3.5 h on agar using 8% saccharin in the hydrogel compared to a vehicle control, a commercial silver-alginate wound dressing and an untreated control (Supplementary Figure S13). As this application showed promising results, we decided to challenge the efficacy of the saccharin hydrogel by applying it on a mature AB5075 biofilm, grown for 24 h, which is more recalcitrant to treatment. The application of the saccharin hydrogel to mature biofilms showed a dose-dependent reduction in the number of viable bacteria, even greater than that obtained with a commercial antimicrobial silver-alginate hydrogel, thus demonstrating the efficacy of this saccharin hydrogel formulation and its potential for clinical applications (Figure 10A). After this test, we progressed to apply it as a wound dressing in an *ex vivo* burn wound model on porcine skin (de Dios *et al*., 2023). A single 1-hour application

of this 6% saccharin hydrogel formulation led to a 1.23-log reduction in bacterial numbers within the wound compared to the unloaded control hydrogel (Figure 10B). These data demonstrates that saccharin retains its antimicrobial activity when loaded in a hydrogel.

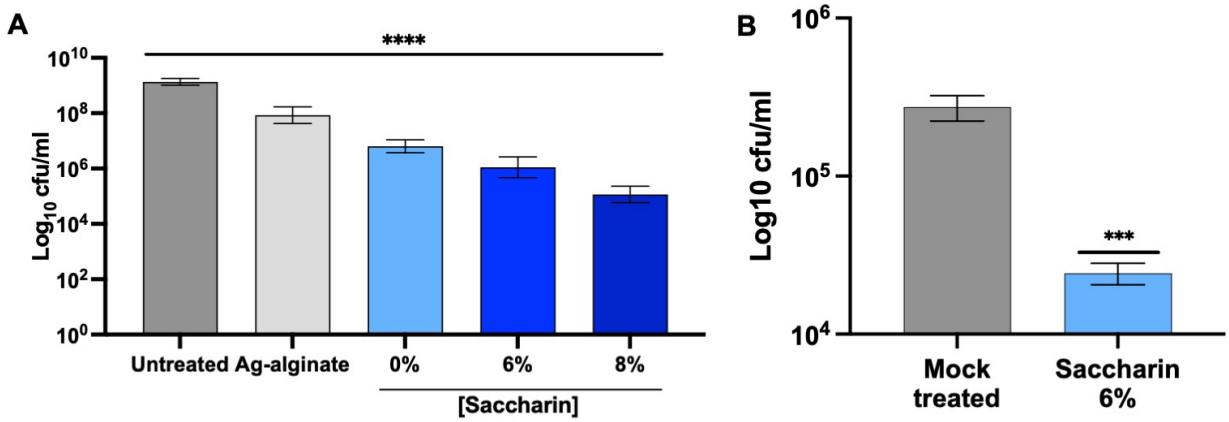

Figure 10. Saccharin shows therapeutic potential in topical treatments: A) Saccharin-loaded hydrogels (6% and 8%) produce a dose-dependent reduction in the bacterial numbers compared to a vehicle control when applied for 1 h on an *A. baumannii* AB5075 colony biofilm grown on an agar plate for 24 hours. B) A 6% saccharin-loaded hydrogel produces a significant reduction in the bacterial numbers compared to a vehicle control in a porcine *ex vivo* burn wound model after a 1-h treatment. Data shown represents the average of three biological replicates ± S.D. Analysis was performed by one-way ANOVA with Tukey's correction for panel A and Student's t-test for B (*** p = <0.001, **** p = <0.0001).

Discussion

Saccharin has been used as a sugar substitute in the human diet for over a century. However, its safety for human health has remained a matter of controversy. In spite of this, it is used as an artificial sweetener worldwide, being the most consumed sweetener in relation to its sweetening power (Sylvetsky and Rother, 2016). In recent years, an increasing number of studies have linked saccharin to different deleterious effects for human health, including glucose intolerance and inflammatory processes. Interestingly, a common nexus between saccharin and these effects is the gut microbiome, pointing at a direct effect of this sweetener on bacteria (Suez *et al*., 2014, Bian *et al*., 2017, Skurk *et al*., 2023, Del Pozo *et al*., 2022). Nevertheless, despite the unequivocal evidence of the impact of saccharin on the microbiome, its direct effect on the bacterial physiology and its underlying mechanism remains unexplored.

Impact on Bacterial DNA Replication Dynamics

Saccharin exposure triggered a loss of cell morphology and filamentation in an *E. coli* model. Septum formation did not appear to be impacted by saccharin indicating an alternative trigger for cell filamentation (Figure 1B). Filamentation can be triggered by cells being unable to terminate synthesis, thus impeding subsequent chromosomal segregation. When we explored the consequences of saccharin exposure at the transcriptomic level, several genes associated with the cell envelope were differentially regulated, but strikingly, pathways linked to DNA replication and mismatch repair systems appeared significantly upregulated (Table X). This suggested saccharin could be impacting DNA synthesis dynamics within the cell. We confirmed this by demonstrating that saccharin-exposed filamented cells had an increased number of *ori* and *ter* foci. However,

these were in line with what would be expected if cell division had not been inhibited, therefore indicating that the chromosomal replication is continuing unabated in filamented cells (Figure 2). This suggested that DNA synthesis may be taking place at sites other than the origin when cells were exposed to saccharin, which we confirmed this by visualizing an increased DnaN signal in *E. coli* cells encoding a thermosensitive version of the chromosomal *ori*-dependent replication initiation protein DnaA, in which chromosomal replication ceases upon a shift to 42 °C (Rudolph et al., 2009). We further confirmed that non *ori*-initiated DNA synthesis was taking place using the Cas1-LFP reporter. We further demonstrated the specificity of this effect by revealing it was dose-dependent and specific to saccharin as ace-K, another artificial sweetener which can induce filamentation, did not trigger the same pronounced effect. Given the increase in non-*ori* initiated DNA synthesis activity following saccharin treatment (Figure 3), we hypothesised that saccharin might be causing DNA damage. This would be coherent with previous studies showing a saccharin-mediated DNA damage via the COMET assay in mouse bone marrow cells (Bandyopadhyay et al., 2008), saccharin induced sperm DNA fragmentation (Rahimipour et al., 2014) and that this sweetener triggers the SOS DNA repair system and the production of reactive oxygen species in bacteria (Yu et al., 2021, Yu and Guo, 2022). In bacteria, BIR pathways catalyse the initiation of DNA synthesis away from the *ori* to repair DNA lesions, therefore we measure the replication foci numbers in two mutants defective in the BIR pathways (*priB* and *priC*) using the recently developed Cas1-LFP DNA synthesis reporter (Figure 4). This reporter showed a significantly lower foci numbers in the absence of the restart protein PriB and PriC upon saccharin exposure, indicating that saccharin induces DNA synthesis away from the *ori* region in a BIR-dependent manner and aligning with our *E. coli* transcriptomic data. However, it was notable that all our assays to study DNA synthesis dynamics were time-limited as a result of cells lysing. This

indicates that the impact of saccharin on the cell envelope usurps the physiological consequences of altered DNA synthesis dynamics within the current experimental set-up. However, the data does indicate that saccharin is triggering the BIR pathways, involved in DNA repair, which suggests some level of DNA damage caused by this artificial sweetener. This damage and repair dynamic, while non-lethal, is likely to ultimately compromise genome integrity leading to an accumulation of mutations in the chromosome. Future work will focus on identifying what specifically is happening to the bacterial chromosome to trigger this increase in DNA synthesis and uncovering the multi-generational consequences of saccharin exposure on bacterial genome integrity.

Impact on the Cell Envelope

Throughout this work, we have shown different results pointing towards an impact of saccharin on the cell envelope that may explain the filametation phenotype. Our microscopy experiments on *E. coli* have shown that cells filament and eventually lyse due to membrane bulging (Figure 1, Supplementary Video S2). This is a typical signature of β-lactam antibiotics, which target peptidoglycan biosynthesis (Yao et al., 2012). Intriguingly, our transcriptomics dataset comparing *E. coli* cells treated and untreated with saccharin showed an activation of β-lactam resistance pathways (Supplementary Table S2). In *A. baumannii*, we similarly observe a loss in cell morphology, resulting innon-dividing, enlarged spherical cells and characteristic cell bulging after saccharin treatment (Figure 9A, Supplementary Video S4). This behaviour is strikingly similar to that shown by Dorr *et al*. after treating *A. baumannii* with meropenem (Dorr *et al.,* 2015). Further studies by Bailey *et al*. have also shown that mutations disrupting genes involved in peptidoglycan biosynthesis in *A. baumannii* produce "giant cells" that are strongly sensitised to meropenem (Bailey et al., 2019, Bailey et al., 2023). Interestingly, mutation of genes involved in DNA replication impaired cell division and also sensitised to this β-lactam antibiotic (Bailey et al.,

673 2023). This aligns with our findings showing the impact of saccharin on the cell envelope
674 morphology and permeability and its potentiating effect on carbapenems (Figure 9). Interestingly,
675 there were no genes directly associated with envelope stress response pathways differentially
676 regulated in the dRNA-seq analysis performed with *A. baumannii*, which may suggest that the
677 affected envelope-related genes respond to a general remodelling in the global transcription to
678 mitigate the saccharin impact. Additionally, we cannot discard envelope stress responses being
679 activated at post-transcriptional levels, which would not be disclosed by transcriptomics.
680 Interestingly, the analysis of our *A. baumannii* transcriptomics data did not show the same
681 enrichment pattern. This could be due to species-to-species differences in the saccharin sensitivity,
682 whereby DNA replication effects are masked in *A. baumannii* or occur earlier upon exposure.
683 Although further efforts need to be made to fully address its mechanism of action, the conserved
684 impact on the cell envelope of different species reinforces our hypothesis of the β-lactam-like
685 effect of saccharin and opens a new avenue to use as the basis for novel therapeutic approaches.

686 **Therapeutic Potential of Saccharin**

687 Currently, the alarmingly increasing prevalence of antimicrobial resistant infections worldwide
688 has led to one of the most important concerns of our time: the antimicrobial resistance crisis. For
689 this reason, novel therapeutic approaches need to be urgently developed against pathogenic
690 bacteria that have evolved resistance to most of the frontline and last-resort antibiotics. We show
691 that saccharin has potential as a potent antimicrobial and can significantly inhibit the growth of
692 MDR *E. coli*, *S. aureus*, *K. pneumoniae*, *A. baumannii* and *P. aeruginosa.* (Figure 5). We further
693 show that saccharin can inhibit biofilm formation (Figure 6A,B) which is a cause of infection
694 treatment failure. However, a more frequent situation in the clinical setting is that a biofilm has
695 already been formed when an antimicrobial treatment starts. For this reason, we challenged

saccharin to disrupt preformed biofilms of both *A. baumannii* and *P. aeruginosa*, obtaining significant reductions in the biofilm biomass in both cases (Figure 6C). These two species, as well as *S. aureus*, are the most prevalent pathogens isolated from wound infections, an environment in which the most common scenario is the polymicrobial infection (Alvarado-Gomez *et al*., 2018). To further challenge the efficacy of saccharin in disrupting biofilms, we reproduced these assays on polymicrobial biofilms, obtaining significant reductions in the *de novo* biofilm formation and biofilm biomass of preformed biofilms (Figure 7). It is estimated that biofilms produce a global burden of $386.8 billion in the healthcare systems and are associated to a higher rate of treatment failure (Camara *et al*., 2022). In this scenario, the anti-biofilm properties of saccharin can be harnessed to develop new therapeutic strategies that help to increase the efficiency of antimicrobial treatments, increasing the success rate and reducing the costs.

Most antibiotics need to find their way into the cell to produce their antimicrobial effect, crossing the bacterial cell envelope by different uptake mechanisms. This can be a limiting factor in the efficacy of an antibiotic. For example, the membrane impermeability to antibiotics is one of the intrinsic resistance mechanisms of *A. baumannii* (McCarthy *et al*., 2021). Thus, disrupting this barrier can lead to more efficient antimicrobial therapies and potentiate the activity of commonly used antibiotics. In this regard, as saccharin produced an alteration of the cell envelope stability (Figure 1, Figure 9A), we investigated if this could affect the function of the membrane as a barrier. We were able to validate an increased permeability of MDR *A. baumannii* AB5075 cells at sub-inhibitory concentrations of saccharin, which led to an increased uptake of the fluorescently-labelled antibiotics (Figure 9B). To challenge if this would lead to an increased antibiotic sensitivity, we assessed the minimum inhibitory concentration (MIC) of different carbapenems on

719 *A. baumannii* AB5075, which is completely resistant to these last-resort antibiotics (Jacobs *et al*.,
720 2014). The reduction of the MIC to levels below the EUCAST breakpoint for *A. baumannii* to be
721 considered resistant (Figure 9C) highlights the potential of saccharin to be used in combination
722 therapies to increase antibiotic uptake and tackle antibiotic resistant infections.

723 As a final step, we tested the therapeutic potential of saccharin to be used as an antimicrobial. As
724 the concentrations of saccharin with antimicrobial activity can be challenging to implement
725 therapeutically when administered orally or intravenously, we opted to propose saccharin as a
726 topical antimicrobial. To assess the feasibility of saccharin as a topical treatment, we selected an
727 *ex vivo* model of clinically relevant conditions, such as a burn wound (Figure 10B), applying it in
728 as part of a PVA hydrogel formulation. Hydrogels allow a controlled and prolonged release of a
729 treatment on wounds (Firlar *et al*., 2022). However, maintaining the activity of the active
730 compound in the hydrogel for the duration of the treatment can be challenging. In the case of
731 saccharin, we were able to formulate a stable hydrogel that retained the antimicrobial activity.
732 After testing it initially *in vitro*, we successfully applied it on an *ex vivo* burn wound model using
733 porcine skin and simulating a biofilm-associated *A. baumannii* infection (de Dios *et al*., 2023).
734 Together, these pilot *ex vivo* topical applications demonstrate the feasibility of saccharin-based
735 formulations as an inexpensive option for prophylaxis and treatment against wound infections.
736 Future work will explore these formulations in acute and chronic *in vivo* infection models.

737 As the realities of a potential post-antibiotic era are beginning to be seen with the increasing
738 prevalence of pan-drug resistant pathogens in hospitals, the urgent need for novel therapeutics is
739 being exacerbated. Here, we have identified a compound in saccharin with previously
740 unrecognised therapeutic potential, overcoming classical limitations associated with many
741 frontline antibiotics such as the inability to treat established biofilms or to be integrated into

742 hydrogel wound dressings. It also has the capacity to potentiate the activity of frontline antibiotics,
743 resensitising previously resistant bacteria. The future therapeutic development of non-classical
744 antimicrobials such as saccharin is likely to be critical to our capacity to effectively control and
745 treat MDR pathogens in the coming decades.

746

Methods

Bacterial strains and growth conditions

A. baumannii AB5075 (VIR-O phase variant (Chin *et al*., 2018)), *P. aeruginosa* PA14, *E. coli* NCTC 13476*, K. pneumoniae* ST234 *and S. aureus* CCUG 68792 were routinely grown in LB (Miller) broth or agar at 37 °C (180 rpm shaking for broth cultures), unless otherwise stated. When necessary, LB was supplemented with $CaCl_2$ 2 mM and $MgSO_4$ 1 mM. Sodium saccharin (used at the concentrations specified in each experiment) was purchased from Fisher Scientific (catalogue number 10722271). All strains used in this work are listed in Supplementary Table S6.

E. coli K12 derivative strains: construction and expression induction

E. coli K12 AB1157 and MG1655 derivative strains used for microscopy experiments are described in the Supplementary Table S4. Strains were constructed via P1*vir* transductions (Thomason *et al*., 2007) or by single-step gene disruptions (Datsenko *et al*., 2000), as indicated in Supplementary Table S4. For expression of Cas1 fused via a linker to eYFP (named Cas1-LFP for simplicity) and Cas2, we used plasmid pTK135 (Killelea and Dimude *et al*., 2023). Briefly, pBAD-HisA (Invitrogen) was used for expression of Cas1-LFP-Cas2 under control of the arabinose-inducible P_{araBAD} promoter, resulting in the over-expression of both Cas1-LFP and untagged Cas2, allowing formation of functional Cas1-Cas2 complexes that can be visualised in living cells (Killelea *et al*., 2023). For expression of Cas1[R84G]-LFP we used pTK136, which is as pTK135, but with a mutated Cas1 version, as previously described (Killelea and Dimude *et al*., 2023). For the experiments using pTK135 and pTK136, expression was induced by addition of arabinose to a final concentration of 0.1% for 60 min before the cells were imaged, as described below. pCP8

768 is a multicopy pBR322 derivative carrying p*ftsKi-ftsZ-cfp*. The plasmid allows the constitutive low
769 expression of a FtsZ-CFP fusion protein from a weak promoter within FtsK (Wang *et al*., 2005).

770 **Growth and biofilm inhibition assays**

771 Overnight cultures of *A. baumannii* AB5075, *P. aeruginosa* PA14, *E. coli* NCTC 13476*, K.*
772 *pneumoniae* ST234 *and S. aureus* CCUG 68792 were diluted in 96-well plates to OD_{600} 0.1 in LB
773 medium supplemented with saccharin in concentrations ranging from 0.5 - 8% (weight/volume
774 expressed in grams per 100 ml), including a vehicle control for each dilution. Cultures were
775 incubated at 37 °C, 180 rpm for 18 h. Following incubation, planktonic growth was assessed by
776 OD_{600} reading.

777 In the case of *A. baumannii* AB5075 and *P. aeruginosa* PA14 cultures biofilm formation was
778 measured after measuring planktonic growth. Media and planktonic cells were removed from the
779 wells and biofilms were gently washed with deionised water three times. Then, 200 µL of 0.1%
780 crystal violet was added to each well and plates were incubated statically for 10 mins at room
781 temperature. The stain was then removed and wells were washed five times with deionised water.
782 After leaving plates to air-dry, the retained crystal violet was re-solubilised by adding 200 µL of
783 99% ethanol to each well and incubating statically at room temperature for 6 h. Crystal violet was
784 quantified by measuring absorbance at 570 nm.

785 Growth inhibition and biofilm inhibition results represent averages of three biological replicates
786 (three technical replicates per experiment). Statistical analysis was performed comparing to the
787 respective vehicle control of each concentration using two-way ANOVA test with Sidak's
788 correction.

789 **Biofilm disruption Assay**

To assess the ability of saccharin to disrupt established biofilms, overnight *A. baumannii* AB5075 and *P. aeruginosa* PA14 cultures were diluted in 96-well plates to OD_{600} 0.1 in LB medium. Plates were incubated for 18 h at 37 °C, 180 rpm to allow biofilms to form. Following incubation, the growth medium was removed from the wells and biofilms were washed three times with 200 µL of sterile PBS to remove any unbound planktonic cells. Fresh LB medium supplemented with 8% saccharin or vehicle control was added to the wells. Plates were incubated for a further 24 h at 37 °C, 180 rpm. Following this treatment, biofilms were stained with 0.1% crystal violet as detailed above. Reduction in biofilm was represented as a percentage reduction compared to the control. The assay was performed in biological triplicates with 3 technical replicates each. Statistical analysis was performed comparing to the respective vehicle control of each concentration using one-way ANOVA with Dunnett's correction.

Polymicrobial Biofilm Dispersal

To assess the effect of saccharin on biofilm formation by polymicrobial cultures and the ability of saccharin to disrupt established polymicrobial biofilms, biofilm inhibition and biofilm disruption assays were set up as previously detailed with some amendments. For the polymicrobial MBIC experiments cultures of *A. baumannii* AB5075*, P. aeruginosa* PA14 and *S. aureus* CCUG 68792 were co-inoculated in a 1:1:1 ratio into LB containing either 2% or 4% saccharin in a 96-well plate. Plates were then incubated at 37 °C, 180 rpm for 24 hours. Following incubation cultures were removed and biofilm were stained and quantified with crystal violet as previously described.

For biofilm disruption assays, mixed cultures of *A. baumannii* AB5075*, P. aeruginosa* PA14 and *S. aureus* CCUG 68792 (in a 1:1:1 ratio) were co-inoculated into TSB in a 96 well plate and

incubated for 24 h at 37°C, 180 rpm. Following incubation, media was removed from the plates and replaced with fresh LB containing 8% saccharin and incubated for a further 24 h at 37 °C, 180rpm. Following this second incubation, biofilms were stained and quantified with crystal violet as previously detailed.

Biofilm inhibition and biofilm disruption assays involving polymicrobial cultures were performed in biological triplicates with 3 technical replicates each. Statistical analysis was performed comparing to the respective vehicle control using Student's t-test.

RNA sequencing and differential gene expression analyses

To assess transcriptomic changes in *E. coli* after saccharin treatment, we used similar conditions to those used in the microscopy experiments. Briefly, *E. coli* MG1655 overnight cultures were diluted 1/100 (v/v) in 20 ml of fresh LB broth (in biological triplicate per condition) and incubated at 37 °C, 180 rpm until early exponential phase (OD_{600} 0.3). At this point, cultures were treated with a final concentration of 1.4% saccharin or an equivalent volume of water and resumed incubation (37 °C, 180 rpm) for an additional hour. Then, samples were withdrawn and preserved in RNAlater at -80 °C until further processing.

In the case of *A. baumannii* AB5075, overnight cultures were diluted 1/100 (v/v) in 20 ml fresh LB broth supplemented with either 1% saccharin or the matching volume of vehicle control (three biological replicates per condition). The cultures were grown to mid-exponential phase (OD_{600} 0.6 approx.) at 37 °C, 180 rpm. Then, samples were withdrawn, spun down and preserved in RNAlater at -80 °C until further processing.

The total RNA from each sample was purified using the RNAeasy Kit with on-column DNAase digestion (Qiagen). RNA integrity was assessed using a Bioanalyzer (RNA 6000 Nano kit) according to the amplitude and sharpness of the peaks corresponding to the 16S and 23S rRNAs. Samples were further processed for cDNA library preparation and sequencing on an Illumina MiSeq with 12 million reads per sample. Sequencing and downstream bioinformatic analyses were performed at SeqCenter (Pittsburgh, Pennsylvania, U.S.A.). Quality control and adapter trimming was performed with bcl2fastq. Read mapping were performed with HISAT. Differential expression analysis was performed using the DESeq R package and using the *E. coli* MG1655 genome annotation (GenBank accession number U00096.3; Blattner et al., 1997) or *A. baumannii* AB5075-UW genome annotation (GenBank accession number NZ_CP008706.1; Gallagher *et al.*, 2015) as references. To assess the physiological pathways altered by saccharin in *E. coli*, a KEGG pathway analysis was performed using limma's "kegga" functionality (default parameters) (Ritchie et al., 2015), where a significant up- and downregulation was considered with an FDR < 0.05. For *A. baumannii*, the functional enrichment of significantly up- and downregulated gene subsets was assessed by means of a Gene Set Enrichment Analysis using FUNAGE-Pro (v2.0) with default parameters (de Jong *et al*., 2022).

Twitching Assay

The twitching motility of *A. baumannii* AB5075 was assessed on twitching agar (tryptone 10 g/l, yeast extract 5 g/l, NaCl 2.5 g/l, agar 10 g/l) as previously described (de Dios *et al.*, 2023). Briefly, freshly autoclaved twitching agar was supplemented with 1%, 0.5% or 0.25% saccharin, or a vehicle control. 10 ml of the supplemented agar were poured in 90-mm Petri dishes and left to dry

for 10 min next to a Bunsen burner. The twitching plates were stab-inoculated with a pipette tip with independent AB5075 colonies freshly grown on LB agar and incubated at 37 °C for 48 h. Each experimental condition was tested in biological quintuplets. Statistical analysis was performed comparing to the respective untreated control using one-way ANOVA with Dunnett's correction.

Single-image microscopy

Fresh overnight cultures of the *E. coli* strains of interest were diluted 100-fold in fresh LB broth (Miller composition) and incubated with vigorous aeration at 37 °C until OD_{600} reached 0.2. If cells were grown in the presence of plasmids (see section "*E. coli* K12 derivative strains: construction and expression induction"), ampicillin was added to the culture at a final concentration of 50 µg/ml. Upon reaching OD_{600} 0.2, 2 ml samples were transferred into sterile pre-warmed glass tubes and saccharin was added to each tube in the desired concentration. The cells were then incubated for different times as indicated in each figure. For staining of the membrane, 10-nonyl acridine orange (NAO, Invitrogen) was added to the sample to a final concentration of 200 nM and incubated for 5 min at room temperature. For staining of the nucleoid, Hoechst 33342 (Thermo Scientific) was added to the same sample to a final concentration of 10 µg/ml and incubated for 5 min at room temperature as well. The visualisation of origin and terminus areas was achieved by using strain RRL189 (see Supplementary Table S4), which constitutively expresses mCherry-LacI and eCFP-TetR, which in turn bind *lacO240* and *tetO240* operator arrays located in the origin and terminus area of the chromosome, respectively. 1 µl of the sample was then pipetted onto an agarose pad and air-dried. For generation of pads, a 65 µl

(15 × 16 mm) GeneFrame (Thermo Scientific) was added to a conventional microscopy slide. 1% of SeaKem LE agarose (Lonza) was added to 1 × M9 minimal medium (diluted from a 5 × stock, Sigma-Aldrich) and heated until the agarose was completely dissolved. 95 µl of the solution was added into the GeneFrame chamber and the chamber sealed immediately with a conventional microscopy slide. Once set, the top slide was removed and the agarose pad air-dried for 20 min at room temperature and used immediately. Once the sample was added and air-dried, the GeneFrame chamber was sealed by adding a 22 × 22 mm cover slip. Visualisation was done using a Ti-U inverted microscope (Nikon) with a CFI Plan Fluor DLL 100 × objective (Nikon) and an ORCA Flash 4.0 LT plus camera (Hamamatsu). Phase contrast images were taken using a pE-100 single LED wavelength source (CoolLED). For fluorescence, the pE-4000 illumination system (CoolLED) was used. The relevant filters for visualisation of Hoechst 33342, CFP, YFP, NAO and mCherry were DAPI-50LP-A Filter (Hoechst 33342), Zeiss filter sets 47 (CFP) and 46 (YFP/NAO), as well as Nikon TXRED-A-Basic (mCherry). Images were captured using the NIS Elements-BR software V4.51 (Nikon). Postprocessing, such as cropping and rotating, was performed in Adobe Photoshop CC (V24.0.0). For all single image microscopy experiments at least two biological replicates were performed. For foci numbers, cells were counted across a minimum of 3 individual frames per experiment.

Time-lapse microscopy

Fresh overnight cultures of the *E. coli* strains of interest were diluted 100-fold in fresh LB broth (Miller composition) and incubated with vigorous aeration at 37 °C until reaching OD_{600} 0.2. 1 µl of the sample was pipetted onto an agarose pad and air-dried. For generation of pads 65 µl (15 ×

16 mm) GeneFrames (Thermo Scientific™) were used. 1% of SeaKem LE agarose (Lonza) was added to LB broth (Miller composition) and heated until the agarose was completely dissolved. If required, saccharin was added to the molten agarose solution at the required concentration. For *E. coli* experiments, 95 µl of the solution was added into a GeneFrame and the chamber sealed immediately with a conventional microscopy slide. Once the agarose had set, the top slide was removed and the pad air-dried for 20 min at room temperature and used immediately. For *A. baumannii* experiments 5 GeneFrames were stacked on top of each other and added to a conventional microscopy slide. 500 µl of the LB medium containing 1% of SeaKem agarose was added into the chamber of the stacked GeneFrames and the chamber sealed immediately with a conventional microscopy slide. Once set, the top slide was removed and 2 mm wide vents cut into the GeneFrame stack on all four sides. The agarose pad was then air-dried for 20 min at room temperature and used immediately. Once the sample was added and air-dried, the GeneFrame chamber was sealed by adding a 22 × 22 mm cover slip. Cells were visualised using the Ti-U system described above. For time-lapse imaging, the temperature was maintained at 37°C using an environmental chamber (Digital Pixel). Time-lapse stacks were captured using the NIS Elements-BR software V4.51 (Nikon). Movie clips were directly exported to mp4 format. Postprocessing of images, such as cropping and rotating, was performed in Adobe Photoshop CC (V24.0.0).

Antibiotic Uptake and Flow Cytometry

To measure the uptake of antibiotics after saccharin treatment, we used the fluorescently labelled derivative of penicillin, Bocillin (Bocillin™ FL penicllin, ThermoFisher Scientific), a

915 fluorescently labelled derivative of vancomycin (BODIPY^{TM} FL Vancomycin, ThermoFisher
916 Scientific) and a customised fluorescently labelled derivative of neomycin (Neomycin-Cy5,
917 synthesis procedure detailed in Supplementary Methods)) in a flow cytometry-based approach. *A.*
918 *baumannii* AB5075 overnight cultures were diluted 1/50 in 4 ml fresh LB medium and incubated
919 for 1 h at 37 °C, 180 rpm. Cultures were treated with 1.5%, 1% and 0.5% saccharin, as well as a
920 mock treatment during 30 min at 37 °C, 180 rpm. After this incubation, samples were harvested
921 and centrifuged. After removing the supernatant, cell pellets were resuspended in PBS and a final
922 concentration of 5 µM of Bocillin, 5 µM of Vancomycin- BODIPY^{TM} FL or 0.1 µM Neomycin-
923 Cy5 was added (including an unlabelled control). Cell samples were mixed thoroughly and
924 incubated at 37 °C in the dark for 10 min prior to flow cytometry detection. To estimate normal
925 cell size, an unlabelled sample withdrawn from a stationary phase culture (non-dividing cells) was
926 subjected to flow cytometry as well.

927 We performed flow cytometry using a BD FACSAria III Cell Sorter (2015-07-14T, BD
928 Biosciences) equipped with red laser (633nm), yellow-green laser (561 nm) and blue laser (488
929 nm). The blue laser was used to collect the forward scatter (FSC) and the side scatter (SCC)
930 through a photodiode, and the Bocillin-FL/Vancomycin-FL signals through a 530/10 bandpass
931 filter. The yellow-green laser was used to collect the Neomycin-Cy5 signal through a 710/50
932 bandpass filter. The threshold operator was set to 200 on SSC. The PMT voltages were customised
933 for optimal separation of different populations. Instrument setting and data acquisition was
934 performed using BD FACSDiva software (V 9.0). This software and FlowJo (V 10.8.1_CL) were
935 used for data analysis. All samples were run at a flow rate of approximately 1000 events/s.

Unlabelled overnight cultures (non-dividing cells) were used as cell-size control and unlabelled exponential phase cells were used to differentiate labelled and unlabelled populations (Supplementary Figure S11A,B).

Flow cytometry data was represented on a dot plot as Fluorescence-A (Y-axis) against SSC-A (X-axis), indicating probe uptake and cell size, respectively, using the FlowJo software. Normal size and oversized populations (X-axis), as well as labelled and unlabelled populations (Y-axis) were gated in the treated samples using the aforementioned controls as a reference.

Antibiotic Sensitivity Assays

Antibiotic sensitivity tests were performed on Mueller-Hinton (MH) agar plates (pH 7.4) supplemented with $CaCl_2$ 2 mM and $MgSO_4$ 1 mM as previously described (de Dios *et al*., 2023). MH media was supplemented with 1.5% or 1% saccharin, or a mock treatment, poured on 90-mm Petri dishes and left to air-dry. Once solidified, plates were inoculated with an *A. baumannii* AB5075 suspension in PBS (0.5 McFarland units) using a cotton swab. MICs for doripenem, imipenem and meropenem were measured using Etest strips (bioMérieux) according to the manufacturer's instructions. The minimum inhibitory concentration (MIC) values were read after incubating the plates at 37 °C for 24 h. Statistical analyses were performed using two-way ANOVA with Tukey's correction. These assays were performed in biological triplicates.

Preparation of saccharin-loaded hydrogels

To test the topical application of a saccharin formulation, we prepared hydrogels containing it as an active component. Potassium tetraborate (3%, w/w) and polyvinyl alcohol (3%, w/w), as well as sodium saccharin (6% or 8%, w/w) (no saccharin for the mock treatment hydrogels) were added into a beaker and mixed with deionized water. The mixture was placed in a water bath and heated at 80 °C for 3 hours while being swirled with a stirring rod every 1 hour. After obtaining the hydrogels, they were placed in a Petri dish and their shape was normalised with custom-made 3D-printed mould. The mould was 3D-printed in a Mars 2 Pro 2K resin 3D printer (Elegoo). Freshly printed moulds were UV-cured in a Wash & Cure 2.0 chamber (Anycubic).

Colony biofilm hydrogel treatment

1-ml LB agar plates were prepared in a 12-well plate. Overnight cultures of *A. baumannii* AB5075 were diluted to OD_{600} 0.05 in PBS. 5 µl of the diluted AB5075 cell suspension were applied to the surface of the agar and allowed to dry. The agar was incubated for 24 hours at 37 °C to form a biofilm. After the incubation, saccharin-loaded moulded hydrogels with concentrations of 6% and 8% saccharin, a vehicle control and a silver-alginate wound care dressing were applied on the biofilm. An untreated biofilm was also used as a control. Then, the plate was transferred back to the incubator for further 24 hours. The hydrogel/dressing was removed, and the agar and the hydrogel surfaces were washed with 1 ml of PBS to resuspend the biofilm. The washing process was repeated 3 times with the same volume, diluting the collected bacterial suspension and enumerating viable cells. These assays were performed in biological triplicates. Statistical analysis was performed comparing all conditions with one-way ANOVA with Tukey's correction.

977

978 ***Ex vivo* porcine skin assay**

979 The porcine skin obtained from the pig belly was purchased from Fine Food Specialists Ltd, not
980 frozen and free of additives. To mimic an acute burn wound, we followed the protocol described
981 by Alves *et al*. (2018) with modifications from de Dios *et al*. (2023). Briefly, an array that contains
982 20 steel pins (8-mm diameter each) was heated to 140 °C for 1 hour and then placed on a 10 cm^2
983 piece of porcine skin for 1 min. After inflicting the burns, the skin was cut into regular 1.5 cm^2
984 pieces which were placed in individual wells of a 24-well plate. Both sides of the skin sections
985 were sterilized under UV light for 1 h. After sterilisation, the burn wounds were inoculated with 5
986 µl of an *A. baumannii* AB5075 suspension in PBS (OD_{600} 0.05). After allowing the bacterial
987 suspension to air-dry, the burnt pieces of skin were incubated for 3.5 hours at 37 °C to allow the
988 formation of a biofilm. Then, a moulded 6% saccharin hydrogel (prepared as described above) was
989 applied on the burn wounds and they were placed back into the incubator for 1 hour. Following
990 treatment, pieces of hydrogels were removed and wounds were washed with 1 mL of sterile PBS
991 while scraping the wound bed (3 times with the same volume of PBS) to recover the cells from the
992 biofilm. The PBS was then diluted and viable cells enumerated. These assays were performed in
993 biological triplicates. Statistical analysis was performed comparing to the respective control using
994 Student's t-test.

995 **Statistical analyses**

996 Graphs show either populational distributions of individual cell counts or average values ±SD
997 (standard deviation). Data representation and statistical comparisons were performed on GraphPad

Prism 10.1.2 (324) (GraphPad Software, San Diego, California USA, www.graphpad.com). The statistical analysis and *post hoc* corrections applied to each dataset, as well as the number of replicates performed per experiment, are indicated in the respective figure legends and Materials and Methods subsections. Parametric or non-parametric tests were selected depending on the results of normality tests performed on each individual dataset.

Data availability

The transcriptomic datasets generated in this work have been made available at the National Center for Biotechnology Information Gene Expression Omnibus (NCBI GEO) public database under the accession numbers GSE276752 (reviewer access token: kxwncqysnpqlbmj) and GSE238183 (reviewer access token: ebitgukixxsrfon) for *E. coli* and *A. baumannii*, respectively.

The mould 3D printing file has been deposited in the NIH 3D Printing Repository under the accession reference 3DPX-020380.

Acknowledgements

RRMC and EM are supported by the NC3Rs PhD Studentship NC/V001582/1. RRMC and RD are supported by a Biotechnology and Biological Sciences Research Council New Investigator Award BB/V007823/1. RRMC and CP are supported by the Academy of Medical Sciences/the Wellcome Trust/the Government Department of Business, Energy and Industrial Strategy/the British Heart Foundation/Diabetes UK Springboard Award (SBF006\1040). RD received a Research Mobility Award from the Young European Research University Network to collaborate with CSL and visit UiT. The work was supported by joint Research Grants BB/T007168/1 and

BB/T006625-1 from the Biotechnology and Biological Sciences Research Council to CJR and ELB, as well as BBSRC research grant BB/W000393/1 to CJR. The work was further supported by a grant by the North Norwegian Health Trust (HelseNord, HN 1688-23) to CSL. MMH and ALW would like to thank the Tromsø Research Foundation and UiT Centre for New Antibacterial Strategies (CANS) for a start-up grant (TFS project ID: 18_CANS).

Competing interest

Brunel University London holds two priority patents covering the therapeutic use of artificial sweeteners and their use as antibiotic potentiators.

References.

Afzaal, M., Saeed, F., Shah, Y.A., Hussain, M., Rabail, R., Socol, C.T., Hassoun, A., Pateiro, M., Lorenzo, J.M., Rusu, A.V. and Aadil, R.M. (2022) Human gut microbiota in health and disease: Unveiling the relationship, *Frontiers in microbiology,* 13, pp. 999001 Available at: 10.3389/fmicb.2022.999001.

Alvarado-Gomez, E., Perez-Diaz, M., Valdez-Perez, D., Ruiz-Garcia, J., Magaña-Aquino, M., Martinez-Castañon, G. and Martinez-Gutierrez, F. (2018) Adhesion forces of biofilms developed in vitro from clinical strains of skin wounds, *Materials Science & Engineering C,* 82, pp. 336-344 Available at: 10.1016/j.msec.2017.08.028.

1038 Anand, R.P., Lovett, S.T. and Haber, J.E. (2013) Break-induced DNA replication. *Cold Spring*
1039 *Harb Perspect Biol.* 5(12):a010397. doi: 10.1101/cshperspect.a010397.

1040 Anderson, R.L. and Kirkland, J.J. (1980) The effect of sodium saccharin in the diet on caecal
1041 microflora, *Food and cosmetics toxicology,* 18(4), pp. 353 Available at: 10.1016/0015-
1042 6264(80)90188-1.

1043 Anju, V.T., Busi, S., Imchen, M., Kumavath, R., Mohan, M.S., Salim, S.A., Subhaswaraj, P. and
1044 Dyavaiah, M. (2022) Polymicrobial Infections and Biofilms: Clinical Significance and
1045 Eradication Strategies, *Antibiotics (Basel),* 11(12), pp. 1731 Available at:
1046 10.3390/antibiotics11121731.

1047 Bandyopadhyay, A., Ghoshal, S. and Mukherjee, A. (2008) Genotoxicity testing of low-calorie
1048 sweeteners: aspartame, acesulfame-K, and saccharin. *Drug Chem Toxicol*., 31(4):447-57.
1049 Available at: 10.1080/01480540802390270.

1050 Bian, X., Tu, P., Chi, L., Gao, B., Ru, H. and Lu, K. (2017) Saccharin induced liver
1051 inflammation in mice by altering the gut microbiota and its metabolic functions, *Food and*
1052 *chemical toxicology,* 107(Pt B), pp. 530-539 Available at: 10.1016/j.fct.2017.04.045.

1053 Boulangé, C.L., Neves, A.L., Chilloux, J., Nicholson, J.K. and Dumas, M. (2016) Impact of the
1054 gut microbiota on inflammation, obesity, and metabolic disease, *Genome medicine,* 8(1), pp. 42
1055 Available at: 10.1186/s13073-016-0303-2.

1056 Bryan, G.T., Ertürk, E. and Yoshida, O. (1970) Production of Urinary Bladder Carcinomas in
1057 Mice by Sodium Saccharin, *Science (American Association for the Advancement of*
1058 *Science),* 168(3936), pp. 1238-1240 Available at: 10.1126/science.168.3936.1238.

1059 Cámara, M., Green, W., MacPhee, C.E., Rakowska, P.D., Raval, R., Richardson, M.C., Slater-
1060 Jefferies, J., Steventon, K. and Webb, J.S. (2022) Economic significance of biofilms: a
1061 multidisciplinary and cross-sectoral challenge, *NPJ biofilms and microbiomes,* 8(1), pp. 42
1062 Available at: 10.1038/s41522-022-00306-y.

1063 Chamanga, E. (2015) Effectively managing wound exudate, *British journal of community*
1064 *nursing,* Suppl Wound Care(9), pp. S8, S10-S10 Available at: 10.12968/bjcn.2015.20.Sup9.S8.

1065 Charbon, G., Bjørn, L., Mendoza-Chamizo, B., Frimodt-Møller, J. and Løbner-Olesen, A. (2014)
1066 Oxidative DNA damage is instrumental in hyperreplication stress-induced inviability of
1067 Escherichia coli, *Nucleic acids research,* 42(21), pp. 13228-13241 Available at:
1068 10.1093/nar/gku1149.

1069 Chin, C.Y., Tipton, K.A., Farokhyfar, M., Burd, E.M., Weiss, D.S. and Rather, P.N. (2018) A
1070 high-frequency phenotypic switch links bacterial virulence and environmental survival in
1071 Acinetobacter baumannii, *Nature microbiology,* 3(5), pp. 563 Available at: 10.1038/s41564-018-
1072 0151-5.

1073 Clifton, L.A., Skoda, M.W.A., Le Brun, A.P., Ciesielski, F., Kuzmenko, I., Holt, S.A. and
1074 Lakey, J.H. (2015) Effect of Divalent Cation Removal on the Structure of Gram-Negative
1075 Bacterial Outer Membrane Models, *Langmuir,* 31(1), pp. 404-412 Available at:
1076 10.1021/la504407v.

1077 Colquhoun, J.M. and Rather, P.N. (2020) Insights Into Mechanisms of Biofilm Formation in
1078 Acinetobacter baumannii and Implications for Uropathogenesis, *Frontiers in cellular and*
1079 *infection microbiology,* 10, pp. 253 Available at: 10.3389/fcimb.2020.00253.

Conlon, M.A. and Bird, A.R. (2014) The impact of diet and lifestyle on gut microbiota and human health, *Nutrients,* 7(1), pp. 17-44 Available at: 10.3390/nu7010017.

Csakai, A., Smith, C., Davis, E., Martinko, A., Coulup, S. and Yin, H. (2014) Saccharin Derivatives as Inhibitors of Interferon-Mediated Inflammation, *Journal of medicinal chemistry,* 57(12), pp. 5348-5355 Available at: 10.1021/jm500409k.

Datsenko, K.A. and Wanner, B.L. (2000) One-Step Inactivation of Chromosomal Genes in Escherichia coli K-12 Using PCR Products, *Proceedings of the National Academy of Sciences - PNAS,* 97(12), pp. 6640-6645 Available at: 10.1073/pnas.120163297.

de Dios, R., Proctor, C.R., Maslova, E., Dzalbe, S., Rudolph, C.J. and McCarthy, R.R. (2023) Artificial sweeteners inhibit multidrug-resistant pathogen growth and potentiate antibiotic activity, *EMBO molecular medicine,* 15(1), pp. e16397-n/a Available at: 10.15252/emmm.202216397.

De Gregorio, E., Del Franco, M., Martinucci, M., Roscetto, E., Zarrilli, R. and Di Nocera, P.P. (2015) Biofilm-associated proteins: news from Acinetobacter, *BMC genomics,* 16(934), pp. 933 Available at: 10.1186/s12864-015-2136-6.

de Jong, A., Kuipers, O.P. and Kok, J. (2022) FUNAGE-Pro: comprehensive web server for gene set enrichment analysis of prokaryotes, *Nucleic acids research,* 50(W1), pp. 330-336 Available at: 10.1093/nar/gkac441.

Del Pozo, S., Gómez-Martínez, S., Díaz, L.E., Nova, E., Urrialde, R. and Marcos, A. (2022) Potential Effects of Sucralose and Saccharin on Gut Microbiota: A Review, *Nutrients,* 14(8), pp. 1682 Available at: 10.3390/nu14081682.

1101 Dent, L.L., Marshall, D.R., Pratap, S. and Hulette, R.B. (2010) Multidrug resistant Acinetobacter
1102 baumannii: a descriptive study in a city hospital, *BMC infectious diseases,* 10(1), pp. 196
1103 Available at: 10.1186/1471-2334-10-196.

1104 Dowd, S.E., Callaway, T.R., Wolcott, R.D., Sun, Y., McKeehan, T., Hagevoort, R.G. and
1105 Edrington, T.S. (2008) Evaluation of the bacterial diversity in the feces of cattle using 16S rDNA
1106 bacterial tag-encoded FLX amplicon pyrosequencing (bTEFAP), *BMC microbiology,* 8(125)
1107 Available at: 10.1186/1471-2180-8-125.

1108 Durack, J. and Lynch, S.V. (2019) The gut microbiome: Relationships with disease and
1109 opportunities for therapy, *The Journal of experimental medicine,* 216(1), pp. 20-40 Available at:
1110 10.1084/jem.20180448.

1111 Ellison, C.K., Whitfield, G.B. and Brun, Y.V. (2022) Type IV Pili: dynamic bacterial
1112 nanomachines, *FEMS microbiology reviews,* 46(2) Available at: 10.1093/femsre/fuab053.

1113 Fan, Y. and Pedersen, O. (2021) Gut microbiota in human metabolic health and disease, *Nature*
1114 *reviews.Microbiology,* 19(1), pp. 55-71 Available at: 10.1038/s41579-020-0433-9.

1115 Fazli, M., Bjarnsholt, T., Kirketerp-Møller, K., Jørgensen, B., Andersen, A.S., Krogfelt, K.A.,
1116 Givskov, M. and Tolker-Nielsen, T. (2009) Nonrandom Distribution of Pseudomonas aeruginosa
1117 and Staphylococcus aureus in Chronic Wounds, *Journal of clinical microbiology,* 47(12), pp.
1118 4084-4089 Available at: 10.1128/JCM.01395-09.

1119 Firlar, I., Altunbek, M., McCarthy, C., Ramalingam, M. and Camci-Unal, G. (2022) Functional
1120 Hydrogels for Treatment of Chronic Wounds, *Gels,* 8(2), pp. 127 Available at:
1121 10.3390/gels8020127.

1122 Gabrilska, R.A. and Rumbaugh, K.P. (2015) Biofilm models of polymicrobial infection, *Future*
1123 *microbiology,* 10(12), pp. 1997 Available at: 10.2217/fmb.15.109.

1124 Gallagher, L.A., Ramage, E., Weiss, E.J., Radey, M., Hayden, H.S., Held, K.G., Huse, H.K.,
1125 Zurawski, D.V., Brittnacher, M.J. and Manoil, C. (2015) Resources for Genetic and Genomic
1126 Analysis of Emerging Pathogen Acinetobacter baumannii, *Journal of Bacteriology,* 197(12), pp.
1127 2027-2035 Available at: 10.1128/JB.00131-15.

1128 Harding, C.M., Hennon, S.W. and Feldman, M.F. (2018) Uncovering the mechanisms of
1129 Acinetobacter baumannii virulence, *Nature reviews.Microbiology,* 16(2), pp. 91-102 Available
1130 at: 10.1038/nrmicro.2017.148.

1131 Hendrickson, H. and Lawrence, J.G. (2007) Mutational bias suggests that replication termination
1132 occurs near the dif site, not at Ter sites, *Molecular microbiology,* 64(1), pp. 42-56 Available at:
1133 10.1111/j.1365-2958.2007.05596.x.

1134 Hou, K., Wu, Z., Chen, X., Wang, J., Zhang, D., Xiao, C., Zhu, D., Koya, J.B., Wei, L., Li, J.
1135 and Chen, Z. (2022) Microbiota in health and diseases, *Signal transduction and targeted*
1136 *therapy,* 7(1), pp. 135 Available at: 10.1038/s41392-022-00974-4.

1137 Jacobs, A.C., Thompson, M.G., Black, C.C., Kessler, J.L., Clark, L.P., McQueary, C.N., Gancz,
1138 H.Y., Corey, B.W., Moon, J.K., Si, Y., Owen, M.T., Hallock, J.D., Kwak, Y.I., Summers, A., Li,
1139 C.Z., Rasko, D.A., Penwell, W.F., Honnold, C.L., Wise, M.C., Waterman, P.E., Lesho, E.P.,
1140 Stewart, R.L., Actis, L.A., Palys, T.J., Craft, D.W. and Zurawski, D.V. (2014) AB5075, a Highly
1141 Virulent Isolate of Acinetobacter baumannii, as a Model Strain for the Evaluation of
1142 Pathogenesis and Antimicrobial Treatments, *mBio,* 5(3), pp. e01076-e01014 Available at:
1143 10.1128/mBio.01076-14.

Jamal, M., Ahmad, W., Andleeb, S., Jalil, F., Imran, M., Nawaz, M.A., Hussain, T., Ali, M., Rafiq, M. and Kamil, M.A. (2018) Bacterial biofilm and associated infections, *Journal of the Chinese Medical Association,* 81(1), pp. 7-11 Available at: 10.1016/j.jcma.2017.07.012.

Kessler, I.I. and Clark, J.P. (1978) Saccharin, cyclamate, and human bladder cancer. No evidence of an association, *JAMA : the journal of the American Medical Association,* 240(4), pp. 349 Available at: 10.1001/jama.1978.03290040027017.

Killelea, T., Dimude, J.U., He, L., Stewart, A.L., Kemm, F.E., Radovčić, M., Ivančić-Baće, I., Rudolph, C.J. and Bolt, E.L. (2023) Cas1-Cas2 physically and functionally interacts with DnaK to modulate CRISPR Adaptation, *Nucleic acids research,* Available at: 10.1093/nar/gkad473.

Kirketerp-Møller, K., Stewart, P.S. and Bjarnsholt, T. (2020) The zone model: A conceptual model for understanding the microenvironment of chronic wound infection, *Wound repair and regeneration,* 28(5), pp. 593-599 Available at: 10.1111/wrr.12841.

Kockler, Z.W., Osia, B., Lee, R., Musmaker, K. and Malkova, A. (2021) Repair of DNA Breaks by Break-Induced Replication. *Annu Rev Biochem*., 90:165-191. Available at: 10.1146/annurev-biochem-081420-095551.

Kulshrestha, A. and Gupta, P. (2022) Polymicrobial interaction in biofilm: mechanistic insights, *Pathogens and disease,* 80(1) Available at: 10.1093/femspd/ftac010.

Kumar, A., Alam, A., Rani, M., Ehtesham, N.Z. and Hasnain, S.E. (2017) Biofilms: Survival and defense strategy for pathogens, *International journal of medical microbiology,* 307(8), pp. 481-489 Available at: 10.1016/j.ijmm.2017.09.016.

Lee, E.H. and Kornberg, A. (1991) Replication deficiencies in *priA* mutants of *Escherichia coli* lacking the primosomal replication n' protein. *Proc Natl Acad Sci U S A.,* 88(8):3029-32. Available at: 10.1073/pnas.88.8.3029.

Maslova, E., Eisaiankhongi, L., Sjöberg, F. and McCarthy, R.R. (2021) Burns and biofilms: priority pathogens and in vivo models, *NPJ biofilms and microbiomes,* 7(1), pp. 73 Available at: 10.1038/s41522-021-00243-2.

McCarthy RR, Larrouy-Maumus GJ, Meiqi Tan MGC, Wareham DW. Antibiotic Resistance Mechanisms and Their Transmission in Acinetobacter baumannii. Adv Exp Med Biol. 2021;1313:135-153. doi: 10.1007/978-3-030-67452-6_7.

Michel, B. and Sandler, S.J. (2017) Replication Restart in Bacteria. *J Bacteriol*., 199(13):e00102-17. Available at: 10.1128/JB.00102-17.

Mitchell, A.M. and Silhavy, T.J. (2019) Envelope stress responses: balancing damage repair and toxicity, *Nature reviews.Microbiology,* 17(7), pp. 417-428 Available at: 10.1038/s41579-019-0199-0.

Mulcahy, L.R., Isabella, V.M. and Lewis, K. (2014) Pseudomonas aeruginosa Biofilms in Disease, *Microbial ecology,* 68(1), pp. 1-12 Available at: 10.1007/s00248-013-0297-x.

NTP (National Toxicology Program). 2021. Report on Carcinogens, Fifteenth Edition. Research Triangle Park, NC: U.S. Department of Health and Human Services, Public Health Service. https://ntp.niehs.nih.gov/go/roc15 (EndNote XML). DOI: https://doi.org/10.22427/NTP-OTHER-1003

Ogunrinola, G.A., Oyewale, J.O., Oshamika, O.O. and Olasehinde, G.I. (2020) The Human Microbiome and Its Impacts on Health, *International journal of microbiology,* 2020, pp. 1-7 Available at: 10.1155/2020/8045646.

ONeill, J. (2016) *Review on antimicrobial resistance: tackling drug-resistant infections globally: final report and recommendations.* London: Wellcome Trust. Available at: https://www.cabdirect.org/Globalhealth/Abstract/20163354200 (Accessed: 21 July 2023).

Pelling, H., Nzakizwanayo, J., Milo, S., Denham, E.L., MacFarlane, W.M., Bock, L.J., Sutton, J.M. and Jones, B.V. (2019) Bacterial biofilm formation on indwelling urethral catheters, *Letters in applied microbiology,* 68(4), pp. 277-293 Available at: 10.1111/lam.13144.

Prashant, G.M., Patil, R.B., Nagaraj, T. and Patel, V.B. (2012) The antimicrobial activity of the three commercially available intense sweeteners against common periodontal pathogens: an in vitro study, *The journal of contemporary dental practice,* 13(6), pp. 749 Available at: 10.5005/jp-journals-10024-1222.

Roilides, E., Simitsopoulou, M., Katragkou, A. and Walsh, T.J. (2015) How Biofilms Evade Host Defenses, *Microbiology spectrum,* 3(3) Available at: 10.1128/microbiolspec.MB-0012-2014.

Ronish, L.A., Lillehoj, E., Fields, J.K., Sundberg, E.J., Piepenbrink, K.H. and Argonne National Lab. (ANL), Argonne,IL (2019) The structure of PilA from Acinetobacter baumannii AB5075 suggests a mechanism for functional specialization in Acinetobacter type IV pili, *The Journal of biological chemistry,* 294(1), pp. 218-230 Available at: 10.1074/jbc.RA118.005814.

Rudolph, C.J., Upton, A.L. and Lloyd, R.G. (2007) Replication fork stalling and cell cycle arrest in UV-irradiated Escherichia coli, *Genes and Development,* 21(6), pp. 668-681. Available at: 10.1101/gad.417607.

Sandler, S.J., Marians, K.J., Zavitz, K.H., Coutu, J., Parent, M.A. and Clark, A.J. (1999) *dnaC* mutations suppress defects in DNA replication- and recombination-associated functions in *priB* and *priC* double mutants in *Escherichia coli* K-12. *Mol Microbiol.*, 34(1):91-101. Available at: 10.1046/j.1365-2958.

Schumacher, M.A. (2017) Bacterial Nucleoid Occlusion: Multiple Mechanisms for Preventing Chromosome Bisection During Cell Division. *Subcell Biochem*., 84:267-298. Available at: 10.1007/978-3-319-53047-5_9.

Serrano, J., Smith, K.R., Crouch, A.L., Sharma, V., Yi, F., Vargova, V., LaMoia, T.E., Dupont, L.M., Serna, V., Tang, F., Gomes-Dias, L., Blakeslee, J.J., Hatzakis, E., Peterson, S.N., Anderson, M., Pratley, R.E. and Kyriazis, G.A. (2021) High-dose saccharin supplementation does not induce gut microbiota changes or glucose intolerance in healthy humans and mice, *Microbiome,* 9(1), pp. 11-18 Available at: 10.1186/s40168-020-00976-w.

Si, J., Vázquez-Castellanos, J.F., Gregory, A.C., Decommer, L., Rymenans, L., Proost, S., Centelles Lodeiro, J., Weger, M., Notdurfter, M., Leitner, C., Santer, P., Rungger, G., Willeit, J., Willeit, P., Pechlaner, R., Grabherr, F., Kiechl, S., Tilg, H. and Raes, J. (2022) Long-term life history predicts current gut microbiome in a population-based cohort study, *Nature aging,* 2(10), pp. 885 Available at: 10.1038/s43587-022-00286-w.

Skurk, T., Krämer, T., Marcinek, P., Malki, A., Lang, R., Dunkel, A., Krautwurst, T., Hofmann, T.F. and Krautwurst, D. (2023) Sweetener System Intervention Shifted Neutrophils from Homeostasis to Priming, *Nutrients,* 15(5), pp. 1260 Available at: 10.3390/nu15051260.

Sorboni, S.G., Moghaddam, H.S., Jafarzadeh-Esfehani, R. and Soleimanpour, S. (2022) A Comprehensive Review on the Role of the Gut Microbiome in Human Neurological Disorders, *Clinical microbiology reviews,* 35(1), pp. e0033820 Available at: 10.1128/CMR.00338-20.

Suez, J., Korem, T., Zeevi, D., Zilberman-Schapira, G., Thaiss, C.A., Maza, O., Israeli, D., Zmora, N., Gilad, S., Weinberger, A., Kuperman, Y., Harmelin, A., Kolodkin-Gal, I., Shapiro, H., Halpern, Z., Segal, E. and Elinav, E. (2014) Artificial sweeteners induce glucose intolerance by altering the gut microbiota, *Nature (London),* 514(7521), pp. 181-186 Available at: 10.1038/nature13793.

Sünderhauf, A., Pagel, R., Künstner, A., Wagner, A.E., Rupp, J., Ibrahim, S.M., Derer, S. and Sina, C. (2020) Saccharin Supplementation Inhibits Bacterial Growth and Reduces Experimental Colitis in Mice, *Nutrients,* 12(4), pp. 1122 Available at: 10.3390/nu12041122.

Sylvetsky, A.C. and Rother, K.I. (2016) Trends in the consumption of low-calorie sweeteners, *Physiology & Behavior,* 164, pp. 446-450 Available at: 10.1016/j.physbeh.2016.03.030.

Sylvetsky, A.C., PhD, Jin, Y., MS, Clark, E.J., Welsh, Jean A., PhD,MPH, RN, Rother, Kristina I.,MD, MHSc and Talegawkar, S.A., PhD (2017) Consumption of Low-Calorie Sweeteners among Children and Adults in the United States, *Journal of the Academy of Nutrition and Dietetics,* 117(3), pp. 441-448.e2 Available at: 10.1016/j.jand.2016.11.004.

1247 Tacconelli, E., Carrara, E., Savoldi, A., Harbarth, S., Mendelson, M., Monnet, D.L., Pulcini, C.,
1248 Kahlmeter, G., Kluytmans, J., Carmeli, Y., Ouellette, M., Outterson, K., Patel, J., Cavaleri, M.,
1249 Cox, E.M., Houchens, C.R., Grayson, M.L., Hansen, P., Singh, N., Theuretzbacher, U., Magrini,
1250 N., Aboderin, A.O., Al-Abri, S.S., Awang Jalil, N., Benzonana, N., Bhattacharya, S., Brink, A.J.,
1251 Burkert, F.R., Cars, O., Cornaglia, G., Dyar, O.J., Friedrich, A.W., Gales, A.C., Gandra, S.,
1252 Giske, C.G., Goff, D.A., Goossens, H., Gottlieb, T., Guzman Blanco, M., Hryniewicz, W.,
1253 Kattula, D., Jinks, T., Kanj, S.S., Kerr, L., Kieny, M., Kim, Y.S., Kozlov, R.S., Labarca, J.,
1254 Laxminarayan, R., Leder, K., Leibovici, L., Levy-Hara, G., Littman, J., Malhotra-Kumar, S.,
1255 Manchanda, V., Moja, L., Ndoye, B., Pan, A., Paterson, D.L., Paul, M., Qiu, H., Ramon-Pardo,
1256 P., Rodríguez-Baño, J., Sanguinetti, M., Sengupta, S., Sharland, M., Si-Mehand, M., Silver, L.L.,
1257 Song, W., Steinbakk, M., Thomsen, J., Thwaites, G.E., van der Meer, J.W., Van Kinh, N., Vega,
1258 S., Villegas, M.V., Wechsler-Fördös, A., Wertheim, H.F.L., Wesangula, E., Woodford, N.,
1259 Yilmaz, F.O., Zorzet, A. and WHO Pathogens Priority List Working Group (2018) Discovery,
1260 research, and development of new antibiotics: the WHO priority list of antibiotic-resistant
1261 bacteria and tuberculosis, *The Lancet infectious diseases,* 18(3), pp. 318-327 Available at:
1262 10.1016/S1473-3099(17)30753-3.

1263 Takayama, S., Sieber, S.M., Adamson, R.H., Thorgeirsson, U.P., Dalgard, D.W., Arnold, L.L.,
1264 Cano, M., Eklund, S. and Cohen, S.M. (1998) Long-term Feeding of Sodium Saccharin to
1265 Nonhuman Primates: Implications for Urinary Tract Cancer, *JNCI : Journal of the National*
1266 *Cancer Institute,* 90(1), pp. 19-25 Available at: 10.1093/jnci/90.1.19.

1267 Thomason, L.C., Costantino, N. and Court, D.L. (2007) E. coli genome manipulation by P1
1268 transduction, *Current protocols in molecular biology (Print),* Chapter 1, pp. 1.17.1 Available at:
1269 10.1002/0471142727.mb0117s79.

Vickridge, E., Planchenault, C., Cockram, C., Junceda, I.G. and Espéli, O. (2017) Management of E. coli sister chromatid cohesion in response to genotoxic stress. Nature Communications, 8:14618. Available at: 10.1038/ncomms14618.

Vijay, A. and Valdes, A.M. (2022) Role of the gut microbiome in chronic diseases: a narrative review, *European journal of clinical nutrition,* 76(4), pp. 489-501 Available at: 10.1038/s41430-021-00991-6.

Wang, Q., Browman, D., Herzog, H. and Neely, G.G. (2018) Non-nutritive sweeteners possess a bacteriostatic effect and alter gut microbiota in mice, *PloS one,* 13(7), pp. e0199080 Available at: 10.1371/journal.pone.0199080.

Wang, X., Possoz, C. and Sherratt, D.J. (2005) Dancing around the divisome: asymmetric chromosome segregation in Escherichia coli, *Genes & development,* 19(19), pp. 2367-2377 Available at: 10.1101/gad.345305.

WHO (2022) *WHO antibacterial preclinical pipeline review.* Available at: https://www.who.int/observatories/global-observatory-on-health-research-and-development/monitoring/who-antibacterial-preclinical-pipeline-review (Accessed: 21 July 2023).

Windgassen, T.A., Wessel, S.R., Bhattacharyya, B. and Keck, J.L. (2018) Mechanisms of bacterial DNA replication restart. *Nucleic Acids Res.,* 46(2):504-519. Available at: 10.1093/nar/gkx1203.

Yao, Z., Kahne, D. and Kishony, R. (2012) Distinct Single-Cell Morphological Dynamics under Beta-Lactam Antibiotics, *Molecular cell,* 48(5), pp. 705-712 Available at: 10.1016/j.molcel.2012.09.016.

1291 Yu, Z., Wang, Y., Henderson, I.R. and Guo, J. (2022) Artificial sweeteners stimulate horizontal
1292 transfer of extracellular antibiotic resistance genes through natural transformation, *The ISME*
1293 *Journal,* 16(2), pp. 543-554 Available at: 10.1038/s41396-021-01095-6.

1294 Yu, Z., Wang, Y., Lu, J., Bond, P.L. and Guo, J. (2021) Non-nutritive sweeteners can promote
1295 the dissemination of antibiotic resistance through conjugative gene transfer, *The ISME*
1296 *Journal,* 15(7), pp. 2117-2130 Available at: 10.1038/s41396-021-00909-x.

1297 Zuarez-Easton, S., Zafran, N., Garmi, G. and Salim, R. (2017) Postcesarean wound infection:
1298 prevalence, impact, prevention, and management challenges, *International journal of womens*
1299 *health,* 9, pp. 81-88 Available at: 10.2147/IJWH.S98876